Climate Dynamics (2005) 25: 777–800
DOI 10.1007/s00382-005-0075-7

Y. Zhao · P. Braconnot · O. Marti · S.P. Harrison
C. Hewitt · A. Kitoh · Z. Liu · U. Mikolajewicz
B. Otto-Bliesner · S.L. Weber

A multi-model analysis of the role of the ocean on the African and Indian monsoon during the mid-Holocene

Received: 3 December 2004 / Accepted: 5 September 2005 / Published online: 5 October 2005

Abstract We investigate the role of the ocean feedback on the climate in response to insolation forcing during the mid-Holocene (6,000 year BP) using results from seven coupled ocean–atmosphere general circulation models. We examine how the dipole in late summer sea-surface temperature (SST) anomalies in the tropical Atlantic increases the length of the African monsoon, how this dipole structure is created and maintained, and how the late summer SST warming in the northwest Indian Ocean affects the monsoon retreat in this sector. Similar mechanisms are found in all of the models, including a strong wind evaporation feedback and changes in the mixed layer depth that enhance the insolation forcing, as well as increased Ekman transport in the Atlantic that sharpens the Atlantic dipole pattern. We also consider changes in interannual variability over West Africa and the Indian Ocean. The teleconnection between variations in SST and Sahelian precipitation favor a larger impact of the Atlantic dipole mode in this region. In the Indian Ocean, the strengthening of the Indian dipole structure in autumn has a damping effect on the Indian dipole mode at the interannual time scale.

Y. Zhao · P. Braconnot (✉) · O. Marti
IPSL/Laboratoire de Sciences du climat et de l'environnement, Unité mixte CEA-CNRS, Orme des Merisiers, bât. 712, 91191 Gif-sur-Yvette, France
E-mail: Pascale.Braconnot@cea.fr

S.P. Harrison
School of Geographical Sciences, University of Bristol, BS8 1SS Bristol, UK

C. Hewitt
Hadley Centre Met Office, Exeter, UK

A. Kitoh
Meteorological Research Institute, Tsukuba, Japan

Z. Liu
University of Wisconsin-Madison, Madison, USA

U. Mikolajewicz
Max Planck Institute für Meteorology, Hamburg, Germany

B. Otto-Bliesner
Climate Change Research, National Center for Atmospheric Research, Boulder, USA

S.L. Weber
Royal Netherlands Meteorological Institute, De Bilt, The Netherlands

1 Introduction

The Paleoclimate Modeling Intercomparison Project (Joussaume and Taylor 1995; PMIP 2000), which aims to understand the mechanisms of climate change and test the capability of climate models to represent a climate state different from that of the present day, has focused on the climate of the mid-Holocene (ca 6,000 year BP) in order to examine model sensitivity to changes in incoming solar radiation (insolation). As a consequence of changes in Earth's orbital parameters, mainly precession, the mid-Holocene was characterized by an increase in the seasonal cycle of insolation in the northern hemisphere (NH) and a decrease in the seasonal cycle in the southern hemisphere (SH). NH insolation was increased by about 5% in the summer and decreased by a similar amount in winter. One of the major responses to these changes in forcing is the enhanced hydrological cycle in the tropics, characterized by strengthened summer monsoons (Kutzbach and Otto-Bliesner 1982; Kutzbach and Street-Perrot 1985; COHMAP-Members 1988; Joussaume et al. 1999).

The mid-Holocene simulations performed within the first phase of PMIP (PMIP I) were made with atmospheric general circulation models (AGCMs). Both the vegetation over land and the mean seasonal cycle of sea-surface temperature (SST) were prescribed to be the same as at the present day (see http://www-lsce.cea.fr/pmip). Thus, these simulations only test the sensitivity of the atmosphere and land surface, to changes in insolation. The models produced an expansion of the

Afro-Asian monsoons that is in qualitative agreement with palaeoenvironmental observations, but PMIP I established that the atmospheric response to orbital forcing was not sufficient to explain observed vegetation and hydrological changes (Yu and Harrison 1996; Harrison et al. 1998; Joussaume et al. 1999; Coe and Harrison 2002). These discrepancies between models and data have been attributed to the changes in ocean circulation or land surface cover that were neglected in PMIP I (PMIP 2000). The models produced very different changes from one another over the Asian monsoon regions (Braconnot et al. 2002), although all of them have increased summer rainfall over the Himalayan foothills.

Coupled simulation allows us to test how different models reproduce past conditions over the ocean, and how ocean feedback alters the mean seasonal cycle and interannual variability. Several modeling studies have shown that the ocean feedback introduces a delay in the response to the change in summer insolation (Kutzbach and Liu 1997; Hewitt and Mitchell 1998; Braconnot et al. 2000, 2004). The ocean response lengthens the African monsoon season by enhancing the land–sea contrast in spring and favoring a northward position of the intertropical convergence zone (ITCZ) over the tropical Atlantic in autumn (Braconnot et al. 1999, Wohlfahrt et al. 2004).

In this paper, we analyze the response to insolation forcing over the tropical ocean in more depth, using seven coupled ocean–atmosphere simulations. We discuss how changes in surface ocean characteristics affect the African and Asian summer monsoons, highlighting systematic differences from the PMIP I simulations, and identify features that are shown by all the models and thus should be a focus for model evaluation during the second phase of PMIP (PMIPII Harrison et al. 2002; Braconnot et al. 2003).

Coupled simulations also provide the opportunity to analyze changes in interannual variability. Previous modeling studies of the early- or mid-Holocene have reported differences in ENSO characteristics and teleconnections compared to the present day (Otto-Bliesner 1999; Liu et al. 2000; Braconnot 2004). Here, we document simulated changes in variability over the Sahel and the Indian Ocean. No climate model reproduces all aspects of the observed modern behavior in the tropical ocean regions (Latif et al. 2001; Davey et al. 2002). We investigate whether, despite these discrepancies, models exhibits similar changes in variability when mid-Holocene insolation forcing is applied.

We focus on the mechanisms of climate change and the role of the ocean in these changes. We do not attempt to make a systematic evaluation of the realism of these simulations because there is neither an up-to-date compilation of mid-Holocene palaeoceanographic data covering the tropical oceans nor a pan-tropical compilation of data on variability changes. Although there has been a substantial increase in the number of marine records describing the changes in oceanic conditions during the Holocene in recent years (e.g. Wang et al. 1999; deMenocal et al. 2000), they are derived from a suite of different proxies and from cores with substantially different temporal resolution—a careful evaluation of these data would be required before they can be used in any systematic way for model evaluation (see e.g. Kohfeld et al. 2005).

The paper is organized as follows: Sect. 2 presents the models used and the characteristics of the simulated climate for present day and mid-Holocene; the coupled simulations over the tropical Atlantic Ocean are discussed in more detail in Sect. 3 and the Indian ocean in Sect. 4; Sect. 5 presents the conclusions of this study.

2 Overview of model simulations and simulated changes for mid-Holocene

2.1 Models and experiment

Each of the seven climate models used in our analyses is made by coupling an atmospheric general circulation model (AGCM) with an ocean general circulation model (OGCM). The two components exchange information about the boundary conditions at the air–sea interface (momentum, heat and fresh water fluxes as well as sea ice). The coupled simulations were performed with models of different resolution and complexity (Table 1). Although most of the models have a full three-dimensional OGCM, the ECHAM3/LSG model has a large-scale geostrophic ocean which does not include all the complexity needed to represent all aspects of the equatorial circulation. ECBILT includes a fully three dimensional OGCM, but has an atmosphere based on the quasi-geostrophic equations. There is a diagnostically computed correction for the ageostrophic terms, which ensures that the large-scale tropical circulation cells are reasonably well simulated. However, regional wind-patterns and the associated ocean currents are not resolved in the tropics. These simplifications make these two models relatively fast but may result in different behavior from the other OAGCMs in the tropical regions.

The simulations of the mid-Holocene follow the PMIP I protocol for insolation changes, including the date of the vernal equinox and the definition of the seasons (Joussaume et al. 1999). Land-surface conditions are, as in PMIP I, the same both in the modern (control) and mid-Holocene experiments. The ECHAM3/LSG model also follows the PMIP I protocol in prescribing a different CO_2 level at 6,000 year BP (280 ppm) from that in the control simulation (380 ppm). All the other models use the same CO_2 level at 6,000 year BP as in the modern control although the actual CO_2 concentration used in both simulations differs from model to model (Table 1). The global energetic of the model is only slightly affected by the changes in orbital parameters; the annual mean change in insolation is negligible (0.011 Wm^{-2}). Most coupled simula-

Table 1 Characteristics of the coupled simulations

MODEL	RESOLUTION		FLUX CORRECTION	CO_2		Reference
	ATM Long × lat (levels)	OCEAN Long × lat (levels)		CTRL	6,000 year BP	
CSM1.2	T31 (18)	102×116 (25)	None	280	280	Otto-Bliesner 1999
UKMO (HADCM2)	96×73 (19)	96×73 (20)	SST, SSS	323	323	Hewitt and Mitchell 1998
IPSL-CM1	64×50 (11)	92×76 (31)	None	345	345	Braconnot et al. 2000
MRI-CGCM1	72×46 (15)	144×111 (23)	SST, SSS,wind	345	345	Kitoh and Murakami 2002
ECHAM3/LSG	T21 (19)	64×32 (11)	SST, SSS	330	280	Voss and Mikolajewicz 2001
ECBILT	T21 (3)	64×32 (12)	None	345	345	Weber 2001
FOAM	R15 (18)	2.8×1.4 (16)	None	345	345	Jacob 1997

Long, lat, levels refer respectively to longitude, latitude and vertical levels. For spectral models, the type of truncation is indicated, whereas for grid point models, the number of grid points is indicated. SST indicates that flux corrections are for sea surface temperature, SSS for salinity, and wind for wind

tions published so far show almost no or very little annual mean change in deep-water formation in the north Atlantic. Changes in CO_2, however, have a larger impact on the global energetic and thus longer runs are required to have confidence in the results. The difference in CO_2 corresponds to an additional mean forcing of -0.88 Wm^{-2}.

We do not have access to the same amount of data for all the simulations. We have the PMIP I standard atmospheric variables (http://www-lsce.cea.fr) for all of the models, except ECHAM/LSG and FOAM. For these two models, features of monsoon activities at mid-Holocene have been reported by Liu et al. (2003) and Mikolajewicz et al (2003). Data are available for the structure of the ocean (mainly temperature, salinity, mixed layer depth, surface currents) from the CSM1.2, IPSL-CM1, MRI-CGCM1 and ECBILT models, but we only have data for individual years of monthly mean values for ocean and atmospheric variables for 50, 70 and 40 years respectively from CSM1.2, IPSL-CM1 and MRI-CGCM1. Thus, we have results from at least three models for every diagnosis, and can use additional information from the other models when appropriate.

2.2 Simulations of present day climate

The large-scale features of modern climatology have been reported for each model (Jacob 1997; Hewitt and Mitchell 1998; Otto-Bliesner 1999; Braconnot et al. 2000; Weber 2001; Voss and Mikolajewicz 2001; Kitoh and Murakami 2002). Five (CSM1.2, IPSL-CM1, HADCM2, MRI-CGCM1 and ECHAM3/LSG) of the seven models have participated in coupled ocean–atmosphere models intercomparison projects: ENSIP (Latif et al. 2001), which focuses on the simulation of El-Niño/Southern Oscillation (ENSO), and STOIC (Davey et al. 2002), which focuses on tropical ocean regions. In general, the coupled models used here capture most features of the observed tropical climatology and reproduce the large-scale characteristics of the modern monsoon. However, almost all the models fail to simulate the magnitude of the seasonal cycle of SST in tropical regions and the patterns of interannual variability associated with ENSO in the tropical Pacific correctly.

Since the focus of this study is the role of the tropical ocean in the response to the insolation forcing, we summarize how the models reproduce the modern mean seasonal cycle of SST over four regions of the tropical oceans: the northern tropical Atlantic (20–60°W, 10–20°N, NAT), the southern tropical Atlantic (30-0°W, 10-0°S, SAT), the Pacific Warm Pool (110–160°E, 0–20°N, WPL) and the northwestern Indian Ocean (55–75°E, 5–15°N, IND). The simulations are compared to the HadISST dataset (2003), which contains averages for the period 1961–1990, and to the Reynolds (1988) data set, which contains averages for 1985–1990.

The models reproduce the seasonal evolution (annual mean removed) of modern SST in the Atlantic over both NAT and SAT (Fig. 1a, b). Most of the models underestimate the magnitude of the seasonal cycle (3°C for NAT and 3.5°C for SAT). The most extreme example of this is ECBILT, which shows < 2°C for NAT and hardly any seasonal differentiation for SAT. However, FOAM overestimates the magnitude of the seasonal cycles in NAT; SST variations are twice as large as shown by the observations. The timing of the seasonal cycle is also satisfactory, although MRI-CGCM1 and CSM1.2 show a slight (ca 1 month) and ECBILT a large (ca 3 months) shift in the timing of the peaks compared to modern climatology. Stronger model-data bias exist in the other regions, in the Pacific and Indian oceans (Fig. 1 c, d). Over the WPL (Fig. 1c), all the models produce warmer SST during summer and autumn. The observations (thick black curves) show a semi-annual cycle in this region with one peak of about 0.5°C (departure from the annual mean) in June and another in October, whereas the models favor generalized warming during the second half of the year. Significant differences between evolution simulated and observed exist for the northwestern Indian Ocean (IND). This is the region for which inter-model and model-data differences are largest, both with respect to the magnitude and the timing of the seasonal

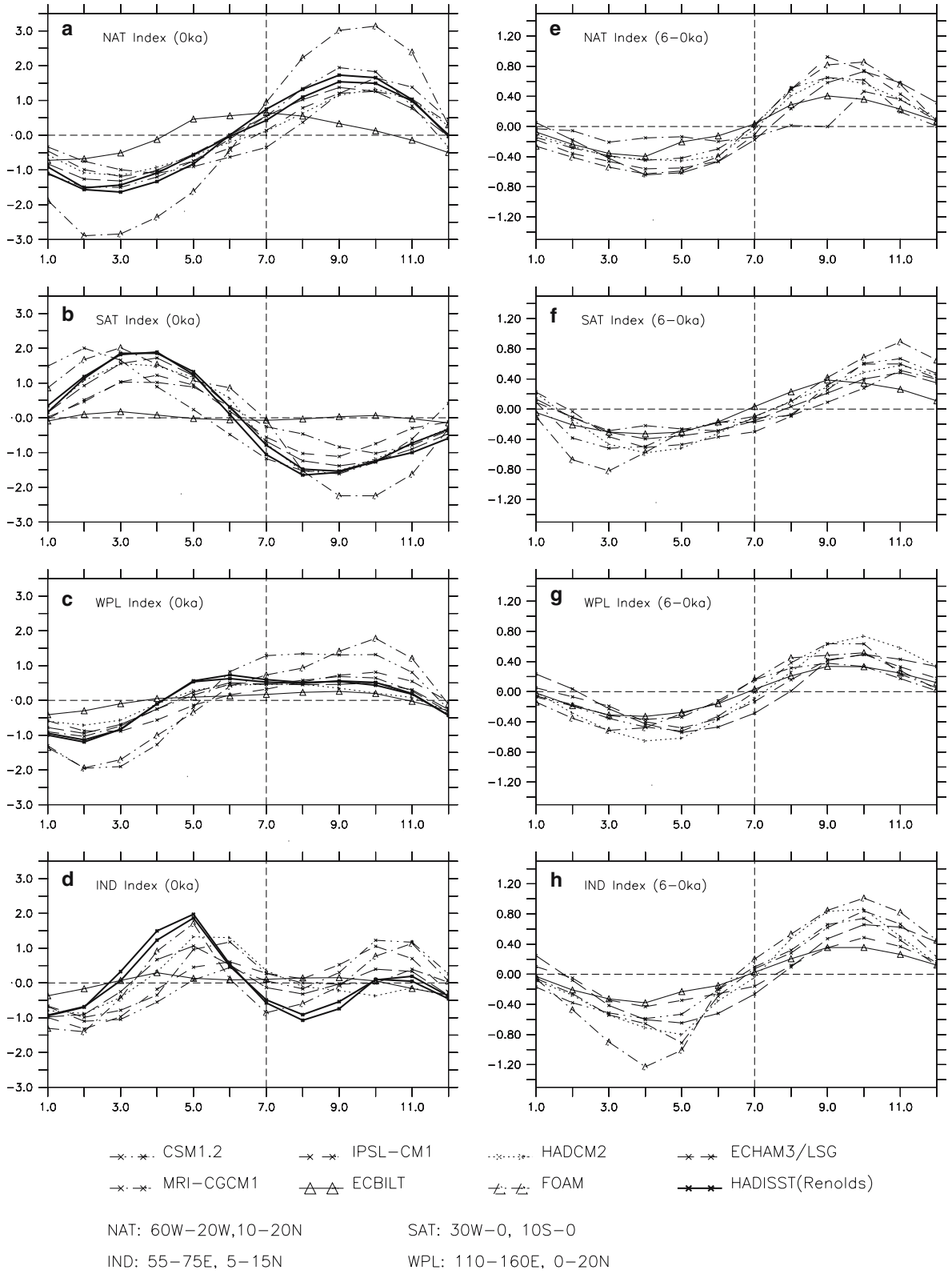

Fig. 1 Comparison of simulated seasonal anomalies (monthly climatology with annual mean removed) of SST for 4 selected regions: **a** north tropical Atlantic ocean (20–60°W, 10–20°N), **b** south tropical Atlantic (30–0°W, 10–0°S), **c** Pacific warm pool (110–160°E, 0–20°N, and **d** Indian Ocean (55–75°E, 5–15°N), for present (control simulations, *left*) and 6 ka—control (*right*). Results from all the coupled models are superimposed on each graph. The 1961–1990 HadSST and 1885–1990 Reynolds SST climatologies are included for comparison

cycle. Nevertheless, the observed spring warming prior to the onset of the Indian monsoon is shown in most simulations, although the magnitude of the warming (2°C) is underestimated by at least a factor of two. Some models simulate the relative warming during October–November but tend to overestimate it by up to 1°C (CSM1.2, IPSL-CM1, FOAM). No model produces the right balance between the two SST maxima.

2.3 Simulation of mid-Holocene climate

The timing of the mean seasonal cycle is altered in response to the mid-Holocene insolation forcing (Fig. 1). All models simulate cooling during the first half-year and warming during the second half-year in all four tropical regions (Fig. 1 e–h). ECBILT captures the change in the seasonal cycle of SST fairly well, although its present-day seasonal cycle is very different from that of the other models. This indicates that the change is a direct response to the insolation forcing, whereas internal dynamics have a large impact on the present-day seasonal cycle. The timing of the largest change reflects the oceanic response to the temporal shift in insolation forcing due to the change in perihelion (Braconnot and Marti 2003). Northern hemisphere insolation peaks in August in the mid-Holocene, but the simulated maximum SST warming is about 2 months later. The warming over SAT is more delayed, because the insolation peak is later at these latitudes. Even through the models show the same behavior, the magnitude of the simulated SST change varies by a factor 2 from one model to another, and the timing is not well defined during winter (Fig. 1). The fact that inter-model differences are larger in winter than summer is because the insolation forcing is smaller and applied over a longer period of time (the time between the autumn and spring equinox increases by 3 days).

To analyse the large-scale features of the changes in surface temperature, precipitation and wind, we present seasonal results from the ensemble mean of seven model simulations. In the northern hemisphere, the mid-Holocene insolation peaks in August and the ocean enhances the summer warming mainly in late summer (Fig. 1). Thus, it is appropriate to define the seasonal mean July, August and September (JAS) as boreal summer and January, February and March (JFM) as boreal winter. All the simulations are interpolated onto a common 3.625° by 3.6° grid. The root mean square (rms) differences between the simulations are computed for each grid point of the common grid.

Boreal winter (JFM) is characterized by a cooling (varies from 1.5 to 4°C depending on the model) over the land in the mid-Holocene simulations compared to the modern control, extending between the equator and 20°N in Africa and to 40°N in East Asia (Fig. 2a). The models show marked cooling in the NAT, whereas the maximum cooling occuring in the Gulf of Guinea or further east is model dependent. Five of the models also show large cooling in the eastern Pacific, in or just south of the region where equatorial upwelling develops or just to the south of it, in the region where some coupled models have a tendency to produce a double ITCZ structure. The cooling in these two regions is associated with a reduction of deep convection and associated precipitation during the mid-Holocene (Fig. 3a). The patterns of temperature change in IND and WPL are different from model to model, although all the models produce a slight cooling over Indonesia and Australia.

The models produce higher temperatures over much of the northern hemisphere land in response to increased summer insolation during boreal summer (Fig. 2b). However, in the region extending from African to India, where monsoon precipitation is increased, there is a slight cooling (Fig. 3b) due to both local recycling (evaporation) and increased cloudiness. This cooling is weaker in the two low-resolution models (ECBILT, FOAM). The simulations produce a large interhemispheric contrast over the ocean, with colder surface temperatures in the southern hemisphere and warmer temperatures in the northern hemisphere. The cold southern hemisphere arises from a combination of insolation forcing and ocean inertia (Liu et al. 2003).

These large-scale temperature changes produce changes in tropical circulation and precipitation patterns. The winter cooling intensifies high pressure and anticyclonic circulation over Asia, Africa and northern South America, enhancing land–sea contrast and thereby reinforcing offshore winds and the export of water from the continent to the ocean. In boreal summer (JAS), the thermal low over Asia and northern Africa is intensified compared to present and favors advection of the moist monsoon flow into the continent and thus increased precipitation (Fig. 3c). In addition, the enhanced inter-hemispheric gradient of temperature enhances the southward shift of the ITCZ over the tropical oceans during winter and enhances the northward shift during summer compared to present.

The large-scale differences in the atmospheric circulation between the mid-Holocene and control coupled simulations are essentially the same as shown by the PMIP I AGCM simulations (Joussaume et al. 1999). However, there are systematic differences between the coupled simulations and the PMIP I simulations that reflect ocean feedback.

3 Atlantic Ocean and African monsoon

3.1 Change in large scale advection of humidity

The highest consistency between the different coupled simulations is found for summer over the Atlantic sector, where most of the models produce a dipole anomaly pattern across 5°N with colder than present SST to the south and warmer SST to the north (Braconnot et al. 2004). Compared to the PMIP I simulations (not shown) the deepening of the continental thermal low extends

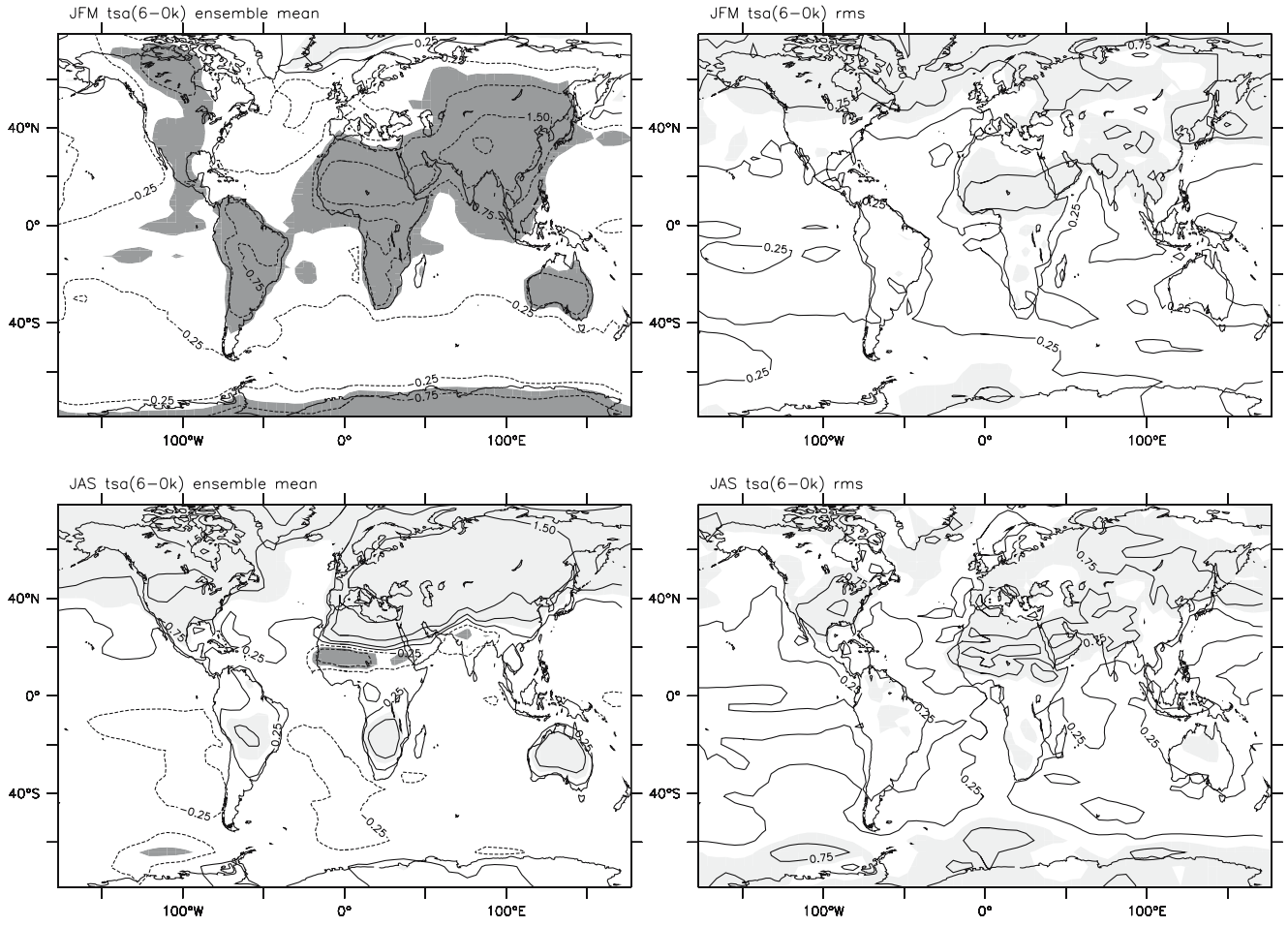

Fig. 2 Simulated changes in **a** winter (JFM) and **b** summer (JAS) surface temperature for mid-Holocene (in °C). Ensemble mean of the seven couple models (*left*) and root mean square difference between simulations (*right*). Isolines are plotted as −5, −3, −1.5, −0.75, −0.25, 0.25, 0.75, 1.5, 3, 5. *Light shading* highlights values higher than 0.5°, and *dark shading* values smaller than −0.5°C

westward over the ocean where temperature are warmer than at present (Fig. 4). In turn, the subtropical Atlantic high shifts to the west and strengthens over the northwestern Atlantic. The easterly 850 hPa wind intensifies from the southern branch of this subtropical high and transports moisture from the warmer northern tropical Atlantic to North America. Precipitation increases over southeastern America (Fig. 3c), which is consistent with reconstructions from pollen and lake data (Harrison et al. 2003). Precipitation decreases over the maritime area occupied by the subtropical high. These large-scale features are also associated with a strengthening of the westerlies between 35 and 40°N along the coast of North America. On the European side, precipitation is reduced over the Iberian peninsula, consistent with a reduction of the northward wind flow from the ocean in these regions. Over northern Africa, southward flow increases in a number of models, resulting in increased advection of warm, moist air from the Mediterranean Sea to the African continent.

The response of Atlantic SST to the insolation forcing reinforces the seasonal march of the ITCZ over the ocean. The maintenance of the ITCZ over the ocean from late summer into autumn sustains active convergence over western Africa and enhances the African monsoon. Change in monsoon rainfall over western Africa is mostly due to moisture advection, and can be estimated from precipitation minus evaporation (P–E). Local recycling is less important during the mid-Holocene than for present day climate (Table 2). Under present-day conditions, P–E accounts for between 12% (ECHAM3/LSG) and 58% (FOAM) of the total precipitation over the region which experiences the maximum precipitation in JAS (20°W–30°E, 10°–25°N). Moisture advection (P–E) accounts for a much larger part (from 36% in ECBILT to 71% in ECHAM3/LSG, average is about 55%) of the increase in mid-Holocene precipitation (Table 2), whereas the change in moisture advection (P–E) accounts for about 45% of the change in precipitation in the PMIP I simulations, (not shown). This indicates that the ocean feedback mainly triggers the land–sea contrast and enhances the advection of moisture from the ocean into the continent. The differences between the model results are the signature of differences in the model set up and parameterization, including interactions between the convection scheme,

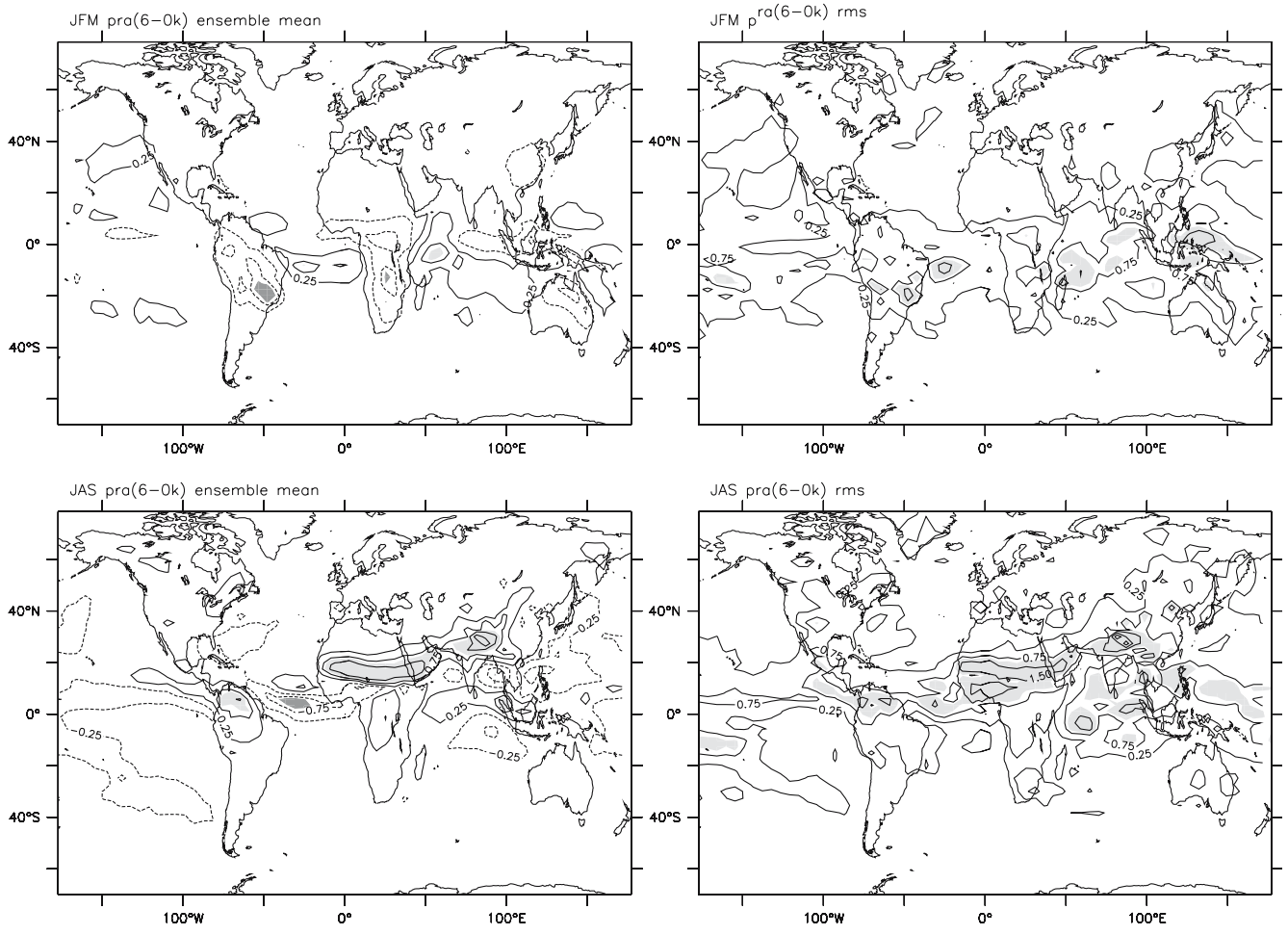

Fig. 3 Simulated changes in **a** winter (JFM) and **b** summer (JAS) precipitation for mid-Holocene (in mm/day). Ensemble mean of the seven couple models (*left*) and root mean square difference between simulations (*right*). Isolines are plotted as −5, −3, −1.5, −0.75, −0.25, 0.25, 0.75, 1.5, 3, 5 mm/day. Light shading highlights values higher than 1mm/day, and dark shading values smaller than −1 mm/day

cloud scheme, boundary layer parameterization, level of complexity of the land surface model, representation of the soil moisture etc.

Palaeoenvironmental evidence shows that the Sahara was wetter during the mid-Holocene than it is today (Street and Grove 1976; Street-Perrott and Perrott 1993; Hoelzmann et al. 1998; Jolly et al. 1998). Lakes, pollen and loess records also indicate wetter conditions over northern India and China (Yu et al. 1998; Kohfeld and Harrison 2000). To compare the coupled simulations with the results of PMIP I simulations, we have averaged the simulated changes in precipitation over the region of Africa (20°W–30°E; 10°N–25°N) used by Joussaume et al. (1999). We only consider the subset of PMIP I simulations that were run with an atmospheric model similar to the one used in the coupled ocean–atmosphere model. This comparison is therefore limited, but it allows some systematic tendencies between AGCM and OAGCM simulations to be identified. The coupled models produce a greater increase in summer precipitation than the PMIP I simulations (Fig. 5). The increase in JAS rainfall ranges from 0.59 mm/day (HADCM2) to 1.36 mm/day (MRI-CGCM1) in the coupled simulations compared to between 0.39 mm/day (HADCM2) and 1.24 mm/day (IPSL-CM1) in the PMIP I simulations. This enhancement is in better agreement with observations, even though the ocean feedback alone is not sufficient to support grasslands as far north as they are known to have occurred in the Sahara (Braconnot et al. 2004).

3.2 Surface fluxes and ocean heat transport as mechanisms to explain interhemispheric changes in SST

Spring cooling and the reinforcement of a dipole SST anomaly across 5°N are two factors that affect both the timing and the northward extent of the African summer monsoon. The question is now to understand how the dipole structure is created and maintained in the simulations. Figure 6a shows the evolution of the

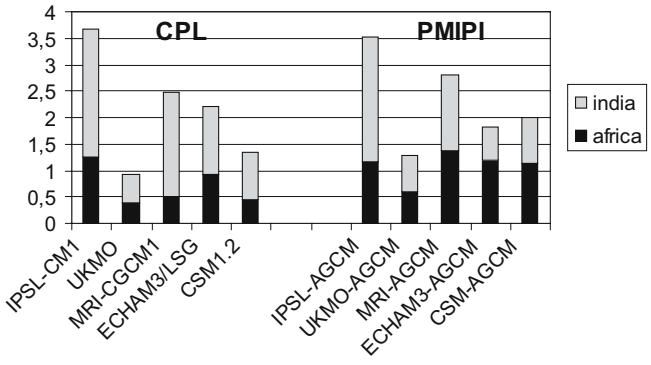

Fig. 4 Change in simulated July–August–September (*JAS*) precipitation averaged over the African monsoon region (20°W–30°E; 10–25°N) and Northern India (70–100°E; 20–40°N) for the coupledsimulations and the equivalent PMIP AGCM simulations

mid-Holocene SST change as a function of time zonal averaged across the Atlantic Ocean for the IPSL-CM1 model. The sharp gradient between the equator and 10°N is present from July to October–November.

The first factor contributing to the surface warming during summer is the increased insolation, which results in increased surface forcing by the net surface heat flux (Fig. 6). The summer increase in net surface heat flux is primarily due to the increase in net solar radiation at the surface, as can be inferred from results of different coupled simulation over the NAT box (Fig. 7). As a result of the distribution of solar radiation with seasons and latitudes, the impact of solar radiation occurs first to the north of the equator and the magnitude increases with latitude. The difference in timing between latitudes contributes to create a differential heating between 20°N and regions located further south, with about one month interval between area north and south of the equator (Fig. 6). The ocean responds with about 1 month lag to this forcing (Fig. 6a). However, insolation alone is not sufficient to create the sharp gradient across 5°N.

The net heat flux is largely controlled by the evaporative feedback between 10 and 20°N (Fig. 7). In this region, evaporation is reduced when temperature increases. Compared to present day, wind speed is reduced in the northwestward trade winds (Fig. 4), which decreases evaporation and thereby enhances the surface warming. This evaporation feedback is twice as large as the net surface insolation forcing during summer. The wind-evaporation feedback is thought to make a major contribution to the decadal climate variations in the tropical Atlantic (Chang et al. 1997). Although there are some analogies between the mid-Holocene simulations and the mechanisms discussed for interannual variability under modern conditions substantial differences are found south of the equator where, unlike in Chang et al. (1997), the wind-evaporation feedback warms the ocean surface.

The only period during which evaporation cools the surface and account for a large amount of the surface heat budget between the equator and 10°N is June (not shown). Therefore, the large delay in the SST response that occurs between the equator and 10°N and contributes to strengthen the dipole structure in late summer cannot be simply explained by an ocean response to surface fluxes. In this region changes in the ocean dynamics and ocean heat transport also play a role (Braconnot et al. 2000). The difference in the meridional heat transport between mid-Holocene and present is directed from the northern to the southern hemisphere from May to October (Fig. 6). This change is located in the surface ocean layers (Fig. 8) and corresponds to the region where surface winds are most affected (Fig. 4). The reversal of the wind between 4 and 10°N (Fig. 4) creates a southward Ekman drift that exports the additional surface heating to the south and delays the local warming.

The evolution of SST as a function of time can be approximated by the evaluation of the mean temperature (T) of the mixed layer (H):

$$\rho\, cH \frac{\mathrm{d}T}{\mathrm{d}t} = Q + \mathrm{div}(uT) + \mathrm{diffusion} \qquad (1)$$

where ρ is density of water, c the heat capacity of water, Q = SWs − LWs − LE − Hs the net surface heat flux at the surface and u the ocean current. The surface heat flux includes the contributions of the net surface short wave (SW, positive downward) and long wave radiations (LW, positive upward), the latent heat flux (LE, positive upward) and the sensible heat flux (Hs, positive upward). Analysis of the contribution of the advection terms to the change in the temperature field for the ocean surface layers using results from the IPSL-CM1 model reveals that these advection terms contribute to cool the region located between 5 and 10°N at a rate that represents 30% of the surface forcing.The differences in the strength of the SST gradient across 5°N amongst the different coupled models thus result from a combination of differences in the surface warming and differences in the strength of the inland monsoon flow. For CSM1.2 and IPSL_CM1, the wind-evaporation feedback and change in the Ekman heat transport are more effective

Table 2 Percentage of JAS precipitation due to water advection, estimated by (P–E)/P averaged over African monsoon region (20°W–30°E, 5–20°N for ECHAM3/LSG and 20°W–30°E, 10–25°N for the other models), as simulated by the different coupled models for the present day (0*k*) and the change between mid-Holocene and present day (6 –0*k*)

MODEL	$(P–E)_{0k}/P_{0k}$	$\Delta(P–E)_{6k\text{-}0k}/P_{6k\text{-}0k}$
CSM1.2	31%	44%
IPSL-CM1	47%	70%
MRI-CGCM1	37%	50%
ECHAM3/LSG	12%	71%
ECBILT	24%	36%
FOAM	58%	61%

Note that evaporation was not available for HADCM2 and so results from this model are not included

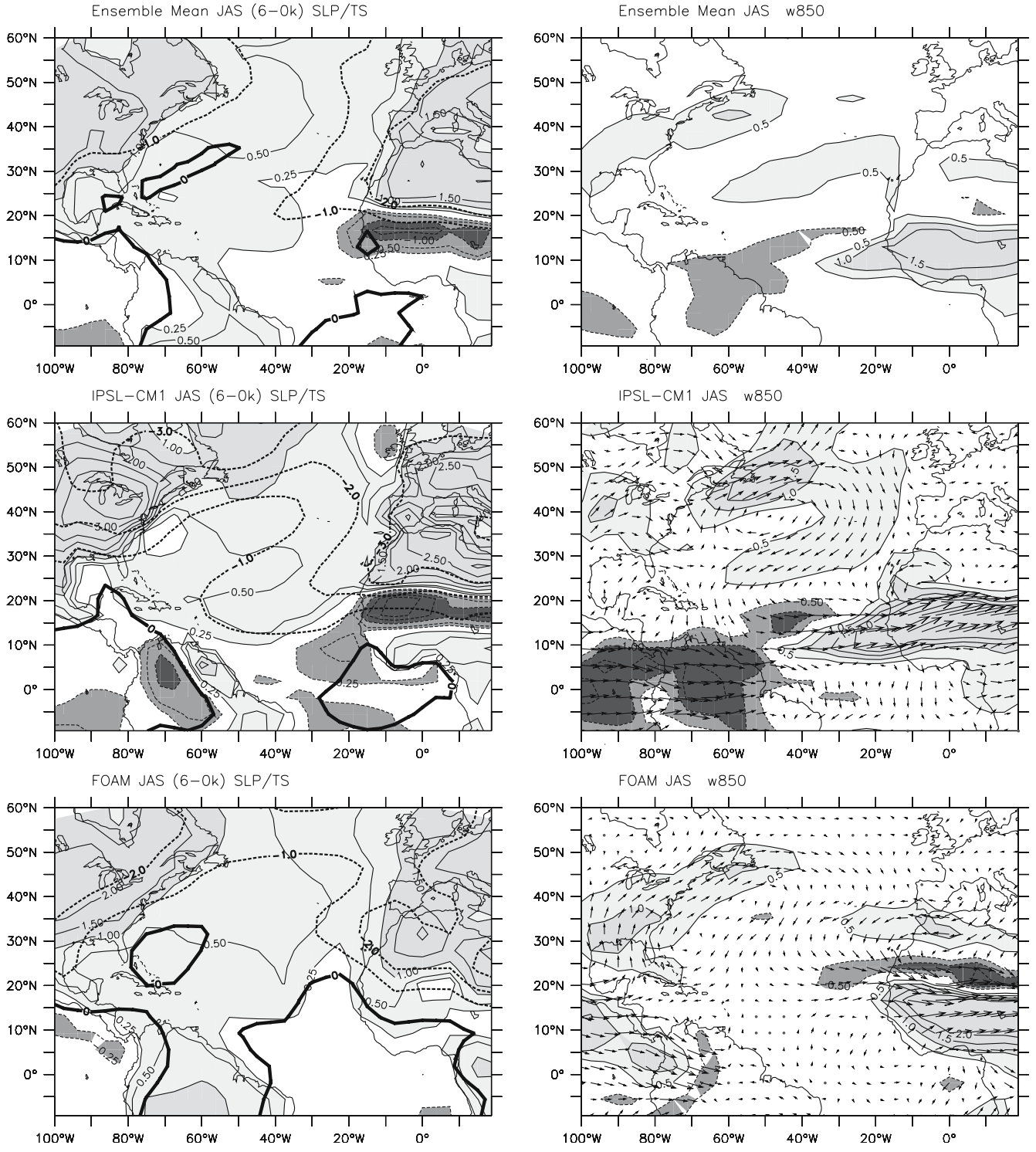

Fig. 5 Simulated surface characteristics during JAS over the tropical Atlantic sector. SLP is a diagnosed variable in ECBILT, and is therefore not included in these analyses. *Left* differences between mid-Holocene and present sea-level pressure (isolines every 1 hPa), superimposed on the surface temperature differences exceeding 0.25°C (−0.25°C) with *light (dark) grey*. Isolines are then plotted every 0.5°C. *Solid lines* stand for positive values and *dotted lines* for negative values. *Right* differences between mid-Holocene and present 850 hPa wind (*arrows*) superimposed on the differences in 850 hPa wind speed. *Light (dark) grey* represents regions where the enhancement (reduction) of wind speed exceeds 0.5 m/s (−0.5 m/s). Isolines are plotted every 0.5 m/s. All *arrows* are referenced to the same scale. For ECBILT model, similar patterns can be found by 850 hPa wind (not shown here). Ensemble mean from six models (*top*) and two models IPSL-CM1 (*middle*) and FOAM (*bottom*)

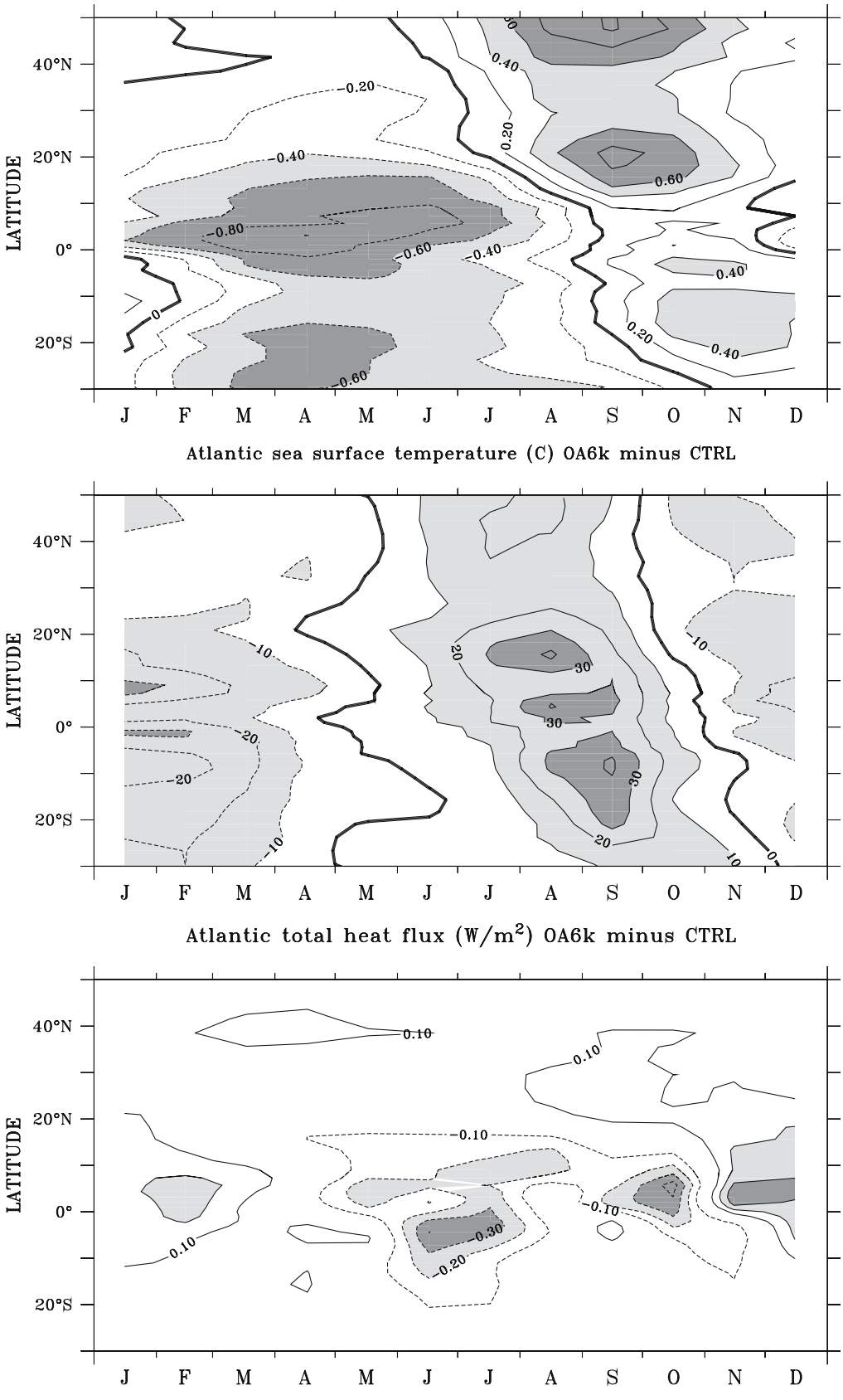

Fig. 6 Hovmöller diagram of the changes as a function of month for the zonal mean tropical Atlantic. *Solid lines* stand for positive values, dashed line for negative values, and heavy line for zero: **a** SST in °C (*dark shading* represent values exceeding 0.6°C and less than −0.6°C, *light shading* represent values greater than 0.4°C and less than −0.4°C), **b** surface heat flux (*dark shading* stand for values greater than 30 W m^{-2} and less than −30 W m^{-2}, and light shading for values greater than 0.4°C and less than −0.4°C); and **c** the integrated meridional heat transport over the top 100 ocean meters for the IPSL-CM1 model (*dark shading* for values greater than 0.3 PW and less than −0.3 PW, light shading for values greater than 0.2 PW and less than −0.2 PW)

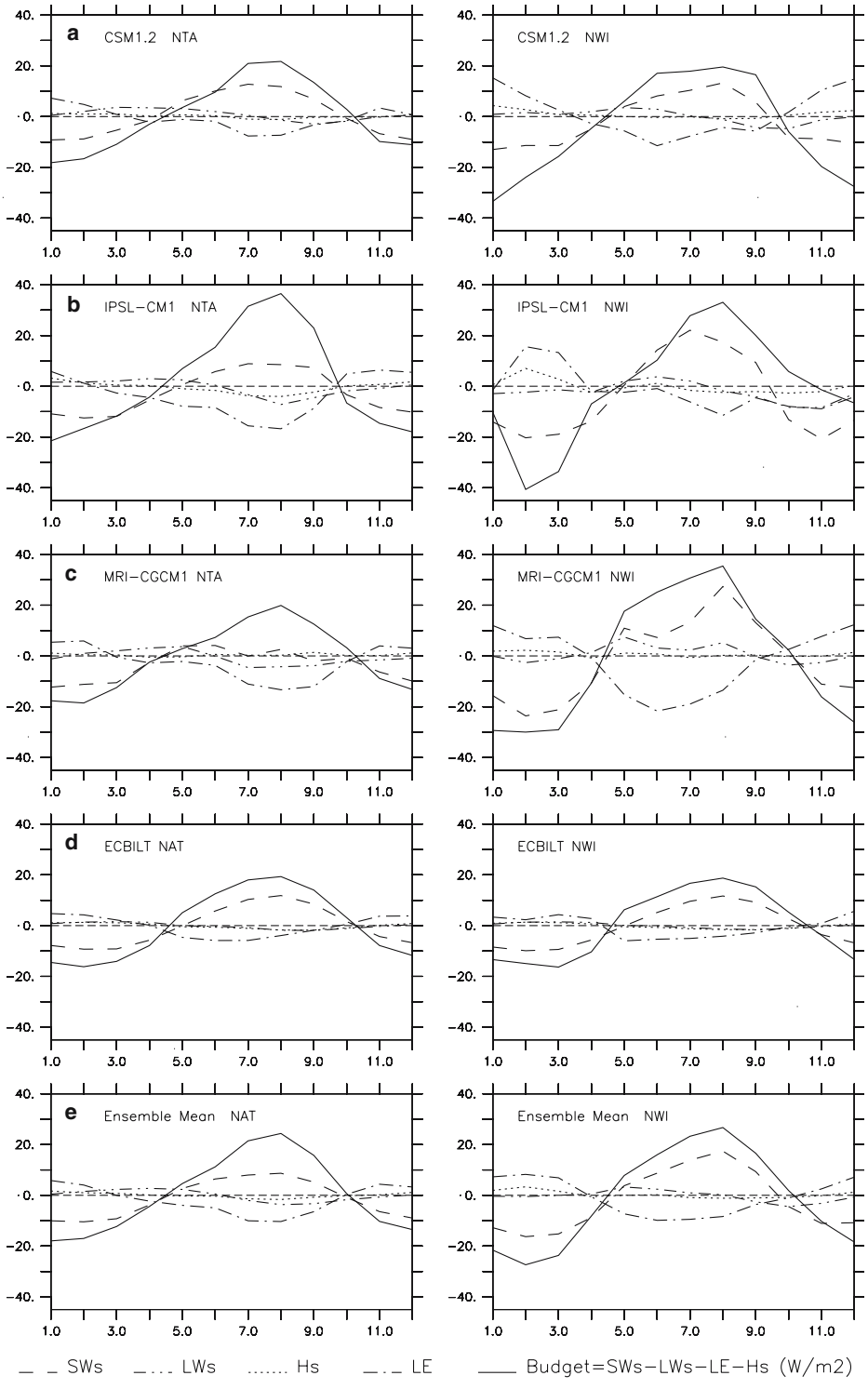

Fig. 7 Changes in surface heat fluxes (Wm^{-2}) for the northern tropical Atlantic ocean (20–60°W, 10–20°N) (*left*) and the northwestern Indian ocean (55–75°E, 5–15°N) (*right*) as simulated by **a** the CSM1.2 and **b** the IPSL-CM1, and **c** the MRI and **d** ECBILT models. Surface heat fluxes include the net solar radiation at the surface (SWs, positive downward), the net longwave radiation at the surface (LWs, positive upward), the latent heat flux (LE, positive upward), the sensible heat flux (Hs, positive upward), and the net heat flux at the surface (budget = SWs–LWs–LE–Hs, positive downward)

than in the other simulations, and the dipole SST pattern across 5°N is well marked. The pattern is more diffuse in the other simulations.

3.3 Interannual variability and Sahel precipitation

Precipitation over West Africa and the Sahel shows considerable interannual variability. Under modern conditions, West African monsoon precipitation increases when the ITCZ is further north than average and/or when the intensity of the convection inside the ITCZ is greater (Janicot 1992). Interannual and decadal variability of summer Sahel rainfall is influenced by variations of global and regional sea surface temperature patterns (Folland et al. 1986; Lamb and Peppler 1992; Fontaine and Janicot 1996; Janicot et al. 1996; Vizy and Cook 2001; Rowell 2003), and in particular SST varia-

tions in the tropical Atlantic (Chang et al. 2000; Nicholson and Grist 2001). We can therefore ask whether the reinforcement of the dipole SST structure over the Atlantic at the seasonal time scale during the mid-Holocene has an impact on the variability of West African precipitation.

To examine this, we use the results from CSM1.2, IPSL-CM1, and MRI-CGCM1 for which we have access to a subset of monthly values of key variables. The maximum increase in summer (JAS) precipitation over western Africa is located just to the north of the maximum of the control simulation (Fig. 9), which reflects a slight shift or a northward extension of the ITCZ. Interannual variability of precipitation is slightly reduced between 6 and 14°N in the three coupled models, and increased in the northern part of the ITCZ. This is also a consequence of the northward shift of the climatic zones over western Africa (Fig. 9). However, the change in variability has a smaller impact on precipitation over this region than the change in the mean. According to the results of the IPSL-CM1 model, the increased monsoon activity corresponds to a reduction of low rainfall and an increase of heavy rainfall events (Fig. 10), both for the change in mean precipitation and the change in interannual variability.

To investigate the relationship between variability and surface temperature, we computed the correlation between a rainfall index and surface temperature during the summer (JAS) season. The "Sahel" rainfall index is defined as precipitation averaged over 10°W–10°E, 8–16°N. For MRI-CGCM1, this index is not well defined in the mid-Holocene because this model simulates a westward shift in the region of maximum precipitation between mid-Holocene and present. For CSM1.2 at present day (Fig. 11), there is an out of phase relationship with positive correlations to the south of 13°N related to the warm land surface along the coast of Gulf of Guinea and negative correlations to the north of 13°N where increased clouds and evaporation both reduce the surface temperature. This pattern reflects the strong local recycling in this model. Over the ocean, a significant dipole pattern is found across 10°N. For IPSL-CM1 at present day, a reverse out of phase pattern is found over land with positive correlations to the north of 16°N and negative ones to the south. This pattern suggests that moisture advection plays a dominant role in the variability of monsoon rainfall. Over the Atlantic, a dipole pattern across 10°N can also be identified, but it is not significant.

The correlation patterns found in the mid-Holocene simulations resemble those in the control experiment for each of the models, but some consistent changes can be found. The out of phase patterns shift northward by 2–3° in CSM1.2 and IPSL-CM1, as expected from the northward shift of the seasonal mean (Fig. 10). The correlation with land surface temperatures over the western Sahara is stronger (Fig. 11). Over the East Atlantic, the dipole pattern around 5–10°N is reinforced in both models. This suggests that the dipole structure across the tropical Atlantic has more impact on sub-Saharan rainfall during the mid-Holocene than at present. The magnitude of the interannual variability of the Atlantic dipole does not vary between the mid-Holocene and control simulation. However, the impact of Atlantic SSTs anomalies on West African rainfall is mostly restricted to the west coast. Also, the only consistent patterns between models are also restricted to the tropical Atlantic sector (Fig. 11).

4 Indian Ocean and Asian monsoon

4.1 Large scale changes in summer monsoon circulation connection between the Indian and Pacific oceans

We now investigate how changes in the ocean circulation influence the response of the Indian and South East Asian monsoons. The coupled models produce consistent changes in the large-scale summer monsoon circulation over the Indian Ocean and increased precipitation over the continent (Fig. 3b). There is a connection between the strengthening of the monsoon flow from the warm pool to the East Asian monsoon and the northwestern Pacific subtropical high. The subtropical high is more active and connected to the Indian Ocean by a band of anomalously high pressure along south East Asia. The extension of this band varies from model to model (Fig. 12). These differences can be related to the difficulties in simulating the northwestern Pacific subtropical high which plays a significant role in the East Asian summer monsoon (Tao and Chen 1987). This structure and the strengthening of the pressure gradient between the Pacific ocean and East Asia contribute to enhance the northward flow along the East coast of India and south East Asia.

The models show that the change in the Indian and East Asian monsoon flow is related to a reduction of Hadley-type circulation with, for most models, less surface flow crossing the equator in the Indian ocean north of Madagascar (Fig. 12). The large-scale changes resemble a shift of the Walker-type circulation from the Pacific Ocean toward the Indian Ocean. The anomalous surface flow intensifies over Indonesia, crosses the Indian Ocean along the equator and joins the monsoon flow near the Somali jet. Monsoon winds are thus reduced from the equator to the tip of India. In the northern part of the Indian Ocean, the monsoon flow intensifies in the Arabian Sea and, for CSM1.2 and IPSL-CM1, in the northern part of the Bay of Bengal. Even though models produce similar gross changes, there is no agreement in the location of the maximum change in wind speed (Fig. 12). These results contradict the view that increasing summer insolation in the northern hemisphere increases the Hadley circulation in the Indian Ocean and the cross equatorial moisture flux along the Somali jet (Clemens and Prell 2003). The heat engine of the system during the mid-Holocene is neither the differential heating nor differential evaporation be-

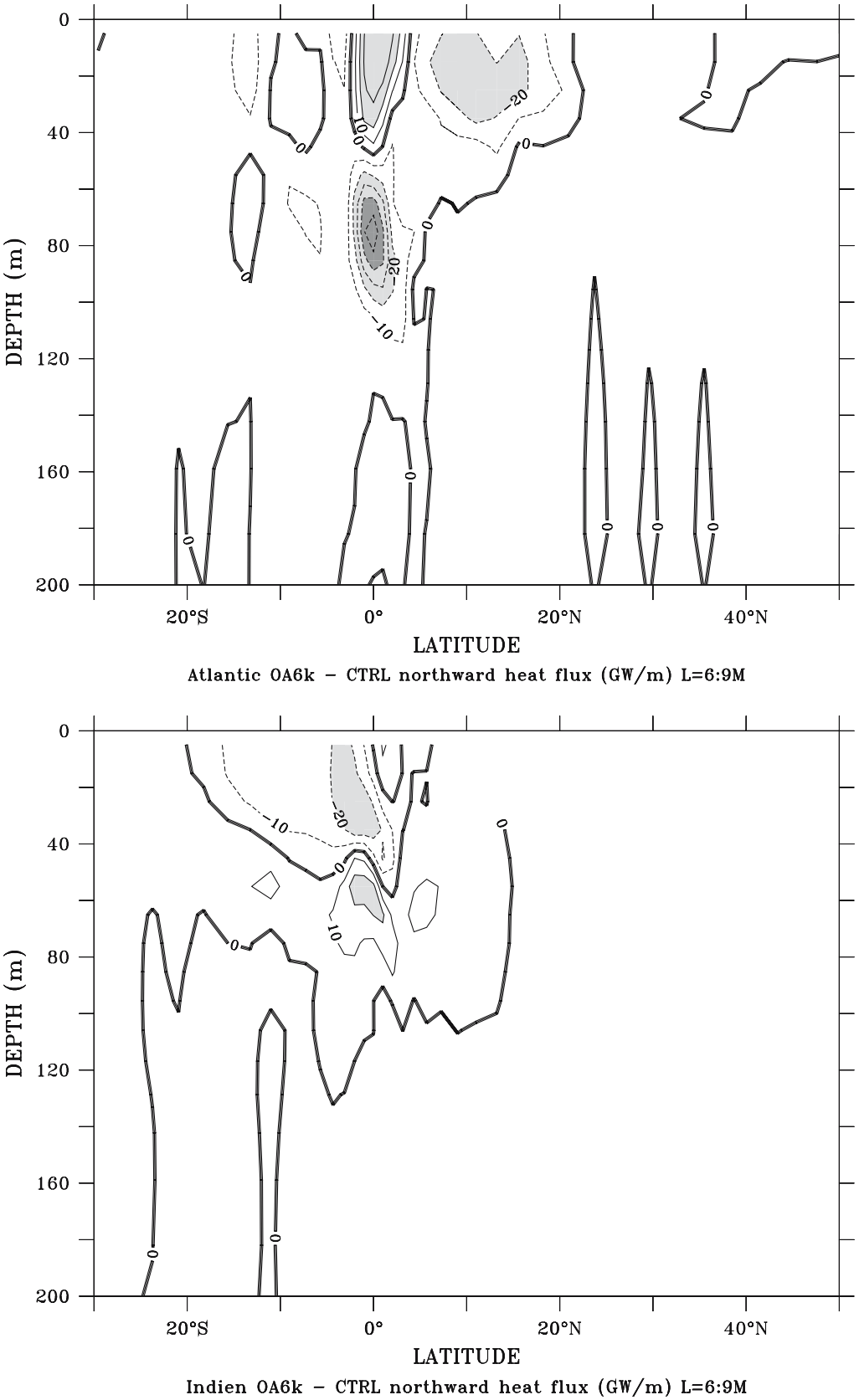

Fig. 8 Change in the meridional heat transport as a function of depth as simulated in **a** the tropical Atlantic Ocean and **b** the tropical Pacific Ocean during summer (JJAS), from the IPSL-CM1 model. *Solid lines* stand for positive values, *dashed* lines for negative values, and the heavy line for zero. *Dark shading* for values greater than 40 GW m^{-1} and less than 40 GW m^{-1}, *light shading* for values greater than 20 GW m^{-1} and less than −20 GW m^{-1}

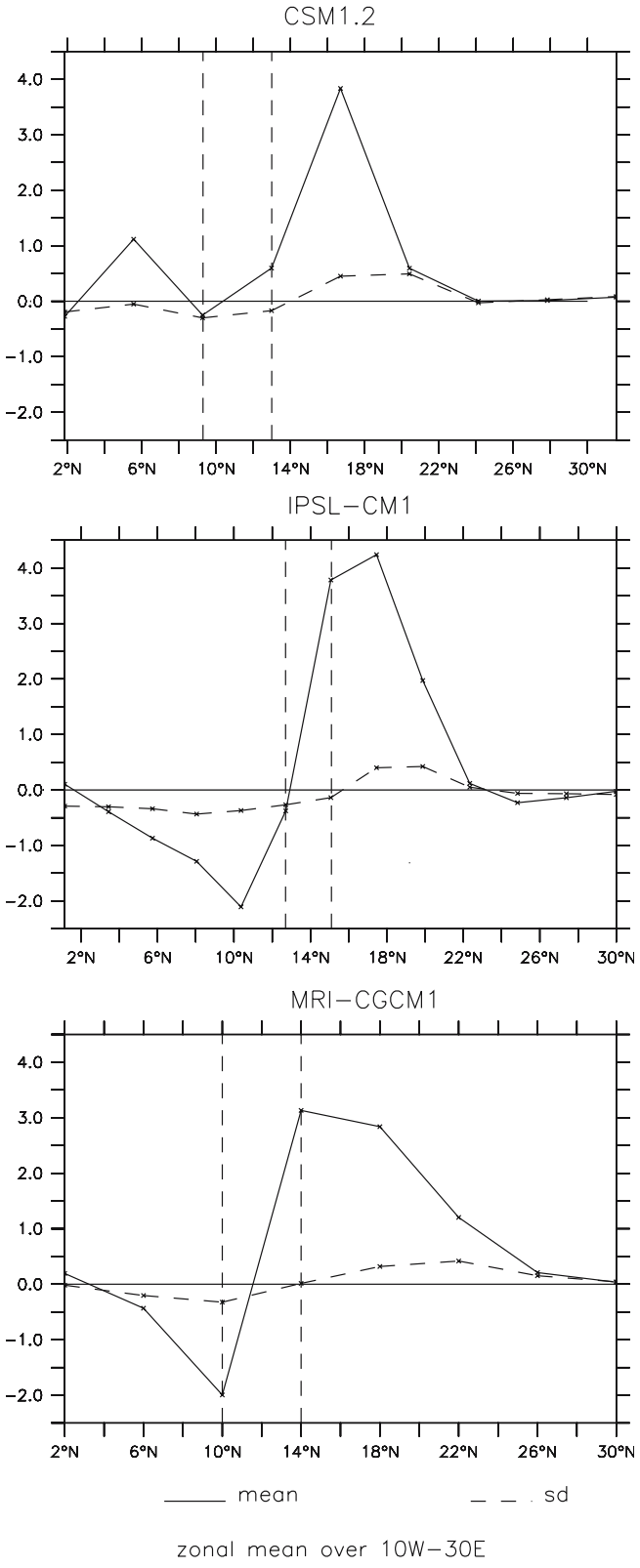

Fig. 9 Mid-Holocene change in precipitation zonally averaged over northern Africa (10°W–30°E) showing both the JAS mean (*solid line*) and the interannual variability (standard deviation; *dotted line*) for CSM1.2, IPSL-CM1 and MRI-CGCM1. On each graph, the *two vertical bars* indicate the location of the maximum precipitation for present day and mid-Holocene respectively

tween the south Indian Ocean and north Indian Ocean, but involves warming of Australia and the associated pressure reduction, which in turn strengthens the low level flow between Australia and the warmer northern hemisphere land. This explains why the change affects the Walker circulation more than the Hadley circulation in this area.

There is no consistency in the simulated monsoon changes over the Indian subcontinent and South East Asia, which may be related to the generally poor representation of the different characteristics of the monsoon in these regions for present day (Zhang et al. 1997; Gadgil and Sajani 1998). Coupled simulations do not systematically increase the change in precipitation in northern India (70–100°E; 20–40°N) compared to the PMIP I simulations. The increase in precipitation varies from 0.64 mm/day (ECHAM3/LSG) to 2.34 mm/day (IPSL-CM1) in the coupled simulations compared to between 0.52 mm/day (HADCM2) and 2.44 mm/day (IPSL-CM1) in the PMIP I simulations. The impact of ocean feedback on this part of the system is difficult to assess because models produce very different pattern of SST changes between the Indian Ocean and the Pacific warm pool (Fig. 2), which locally modify the land–sea contrast and the inland advection of the monsoon flow.

4.2 Late ocean warming causes late monsoon retreat over the northern Indian ocean

Comparison of the coupled simulations and the PMIP I simulations shows that ocean feedback delays ocean warming in autumn over the Indian ocean, south of 20°N (Figs. 12, 13). This pattern of SST change is associated with increased precipitation and an anomalous large-scale convergence of surface winds into the warmer region (Fig. 12). Reduced precipitation occurs to the south, reflecting a northward shift of the ITCZ in the northwestern Indian Ocean. This feature results from ocean-atmosphere interactions. Other variables such as sea surface salinity (SSS) and mixed layer depth also have corresponding responses over this region (Fig. 13). Precipitation increases in late summer when SST warms and salinity decreases in response to the fresh water input at the surface. The depth of the mixed layer increases in winter in response to the surface cooling and shoals by about 8 m in autumn, reaching its most shallow state in September–October when SST is higher and SSS becomes fresher. The evolution of surface temperature, precipitation, SSS and mixed layer depth (Fig. 13) are different but all lag the change in surface heat flux by about 2 months (Fig. 7). Moreover, both surface warming and precipitation stratify the surface ocean and enhance the shoaling of the mixed layer depth. As for the Atlantic Ocean, the most important factor contributing to the surface warming is the increased summer solar radiation. A strong wind-evaporation feedback in this re-

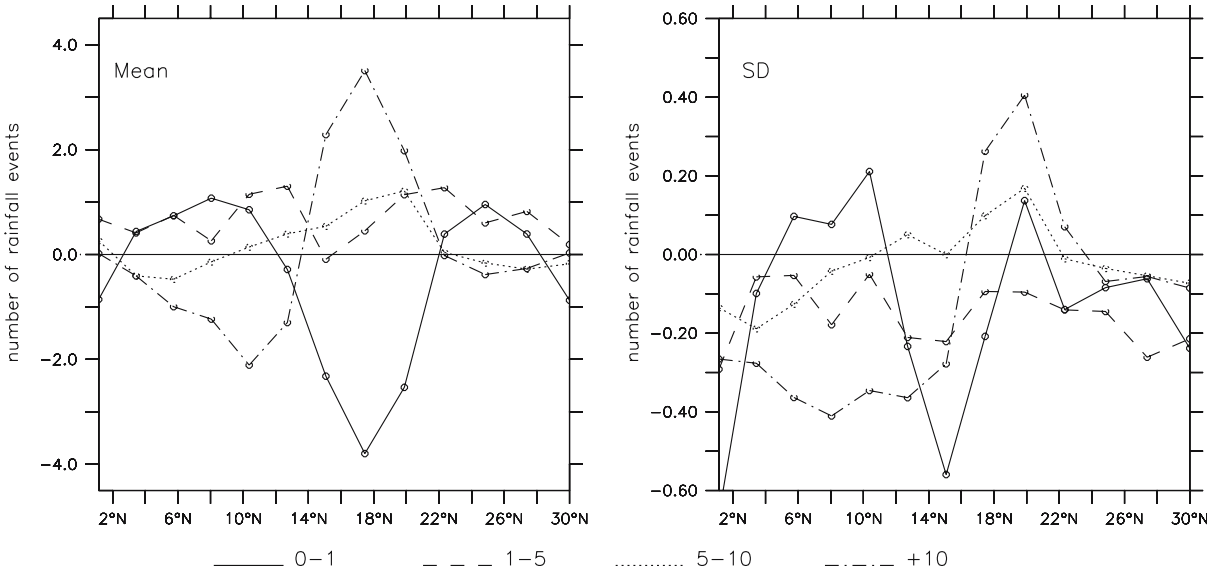

Fig. 10 Mid-Holocene change in precipitation zonally averaged over northern Africa (10°W–30°E) expressed in terms of the number of days in each of four rainfall classes, using results from the IPSL-CM1 model. **a** Change in JAS mean and **b** change in JAS standard deviation. The different classes correspond to rainfall events of < 1 mm/day (*solid line*), between 1 and 5 mm/day (*dashed line*), between 5 and 10 mm/day (*dotted line*) and > 10 mm/day (*dashed-dotted line*)

gion of reduced summer wind speed reinforces the warming (Fig. 7). For most models this feedback is larger than in the Atlantic ocean. However, it is not clear if the change in mixed layer depth has an impact in triggering the autumnal warming.

The possible role of the change in the mixed layer can be analyzed using a very simple model of the mixed layer. Our goal is to establish if the late surface warming and local feedbacks are sufficient to enhance the late surface warming by reducing locally the thermal inertia of the surface ocean. To simplify the problem, we assume that SST is representative of the mean temperature of the mixed layer. We neglect the role of heat transport and upwelling by assuming there is no advection of heat across the boundary of the region and no heat exchange between the mixed layer and deeper parts of the ocean. These assumptions seem reasonable given that there is nearly no change in the surface heat transport in this region (Fig. 8). We then analyse successive equilibrium states.

With the above assumptions, the thermodynamic Eq. 2 controlling the rate of warming of the mixed layer reduces to:

$$\frac{\mathrm{d}T}{\mathrm{d}t} = \frac{Q}{\rho c H}. \tag{2}$$

For a given time interval (month or season), the difference of warming rate between mid-Holocene ($6k$) and present ($0k$) is given by

$$\left(\frac{\mathrm{d}T}{\mathrm{d}t}\right)_{6k} - \left(\frac{\mathrm{d}T}{\mathrm{d}t}\right)_{0k} = \frac{1}{\rho c}\left(\frac{Q_{6k}}{H_{6k}} - \frac{Q_{0k}}{H_{0k}}\right). \tag{3}$$

When changes in the mixed layer depth are neglected, this equation reduces to

$$\left(\frac{\mathrm{d}T}{\mathrm{d}t}\right)_{6k} - \left(\frac{\mathrm{d}T}{\mathrm{d}t}\right)_{0k} = \frac{1}{\rho c H_{0k}}\left(Q_{6k} - Q_{0k}\right). \tag{4}$$

We compare the results of these two formulas for the box located over the northwestern Indian Ocean (55–75E, 5–15 N) where the ocean exhibits a late surface warming, in the CSM1.2 and IPSL-CM1 simulations for which we have access to mixed layer depth, temperature and salinity outputs. The net heat flux peaks in August (Fig. 13) and is mainly attributed to the changes of short-wave flux and latent heat cooling. Precipitation increases only from late summer to autumn. This is the time of the year when the change in mixed layer depth is most effective in reducing the surface heat inertia of the water column and contributes to the surface warming. The rate of change of surface temperature is larger when the change in the mixed layer is considered (Fig. 13). For CSM1.2, the late summer warming reaches 0.4°C/month using Eq. 3, which is nearly the simulated value, but only 0.2°C/month with Eq. 4. Similar results can be found with the IPSL-CM1 model. Our analysis thus supports a positive feedback involving the change in mixed layer depth, local warming and precipitation and large-scale atmospheric advection over these warmer waters during the retreat of the monsoon.

The change in mixed layer depth is less effective during winter, when the mixed layer depth deepens, because it corresponds to a period when the mixed layer is deep in the control simulations. If we expand Q_{6k} and H_{6k} as:

$$Q_{6k} = Q_{0k} + \mathrm{d}Q, \tag{5}$$

$$H_{6k} = H_{0k} + \mathrm{d}H. \tag{6}$$

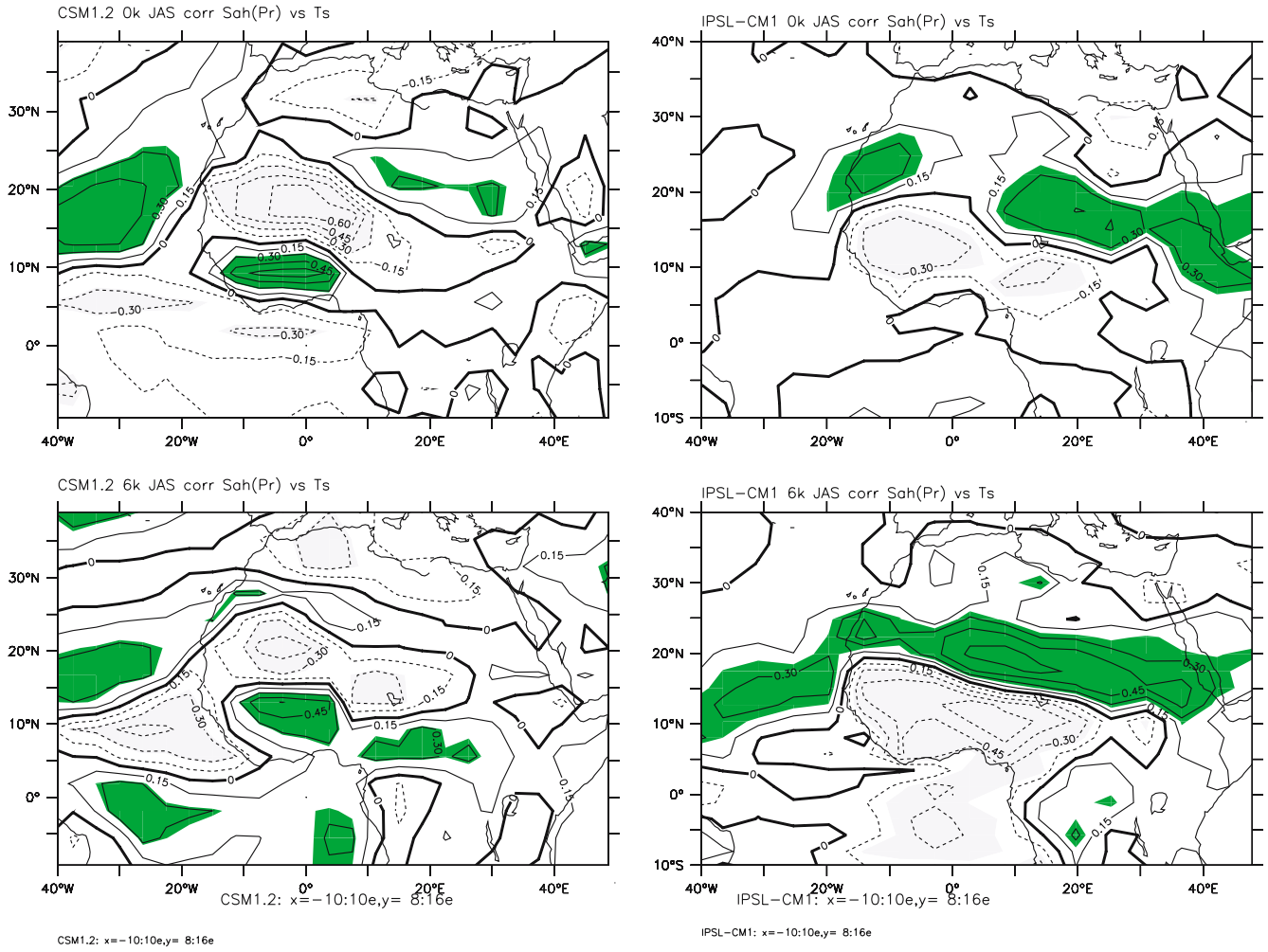

Fig. 11 Correlation patterns between West Sahel index and surface temperature. The West Sahel index is constructed as rainfall averaged over a box extended from 10°W to 10°E, and from 8 to 16°N. *Heavy (light) grey shading* indicates a positive (negative) 5% level of significance. The 5% significant value is 0.28 for CSM1.2 and 0.23 for IPSL-CM1, which corresponds to the difference in the length of the simulation between the two models. Isolines are plotted every 0.15

Then:

$$\left(\frac{\mathrm{d}T}{\mathrm{d}t}\right)_{6k} - \left(\frac{\mathrm{d}T}{\mathrm{d}t}\right)_{0k} = \frac{1}{cH_{0k}} \frac{\left(\mathrm{d}Q - Q_{0k}\frac{\mathrm{d}H}{H_{0k}}\right)}{\left(1+\frac{\mathrm{d}H}{H_{0k}}\right)}. \quad (7)$$

The denominator is larger than 1 for an increase in H and smaller than 1 for a decrease in H, which explains the difference in the role of the mixed layer depth between winter and summer.

4.3 Do changes in the mean seasonal cycle inhibits Indian Ocean dipole variability?

The pattern found across the Indian ocean in autumn bears some resemblance to the Indian Ocean Dipole (IOD) (Webster et al. 1999). At the present day, the IOD is characterized by anomalously low SSTs in the southeastern equatorial Indian Ocean (90–110°E, 10–0°S) and anomalously high SSTs in the western Indian Ocean, with associated wind and precipitation anomalies. The IOD plays a key role in climate change in the tropical Indian Ocean at interannual to longer time scales (Saji et al. 1999; Gadgil et al. 2003). The dipole mode is independent of ENSO and the air-sea interactions involved are unique and inherent to the Indian Ocean (Saji et al. 1999). Since this dipole structure is reinforced during mid-Holocene at the seasonal time scale, we investigate if this has an impact on the characteristics of interannual variability.

Despite the differences in both the simulated mean SST and SST changes over the Indian ocean in the control experiments (see Fig. 3), all three models (CSM1.2, IPSL-CM1 and MRI-CGCM1) show a decrease in the variance of the mid-Holocene dipole mode index (DMI) in autumn compared to present day (Fig. 14). Here DMI is defined as the SST anomaly between the western tropical Indian Ocean (50–70°E, 10S–10°N) and the eastern tropical Indian Ocean (90–110°E, 10S-0). In CSM1.2, the variance

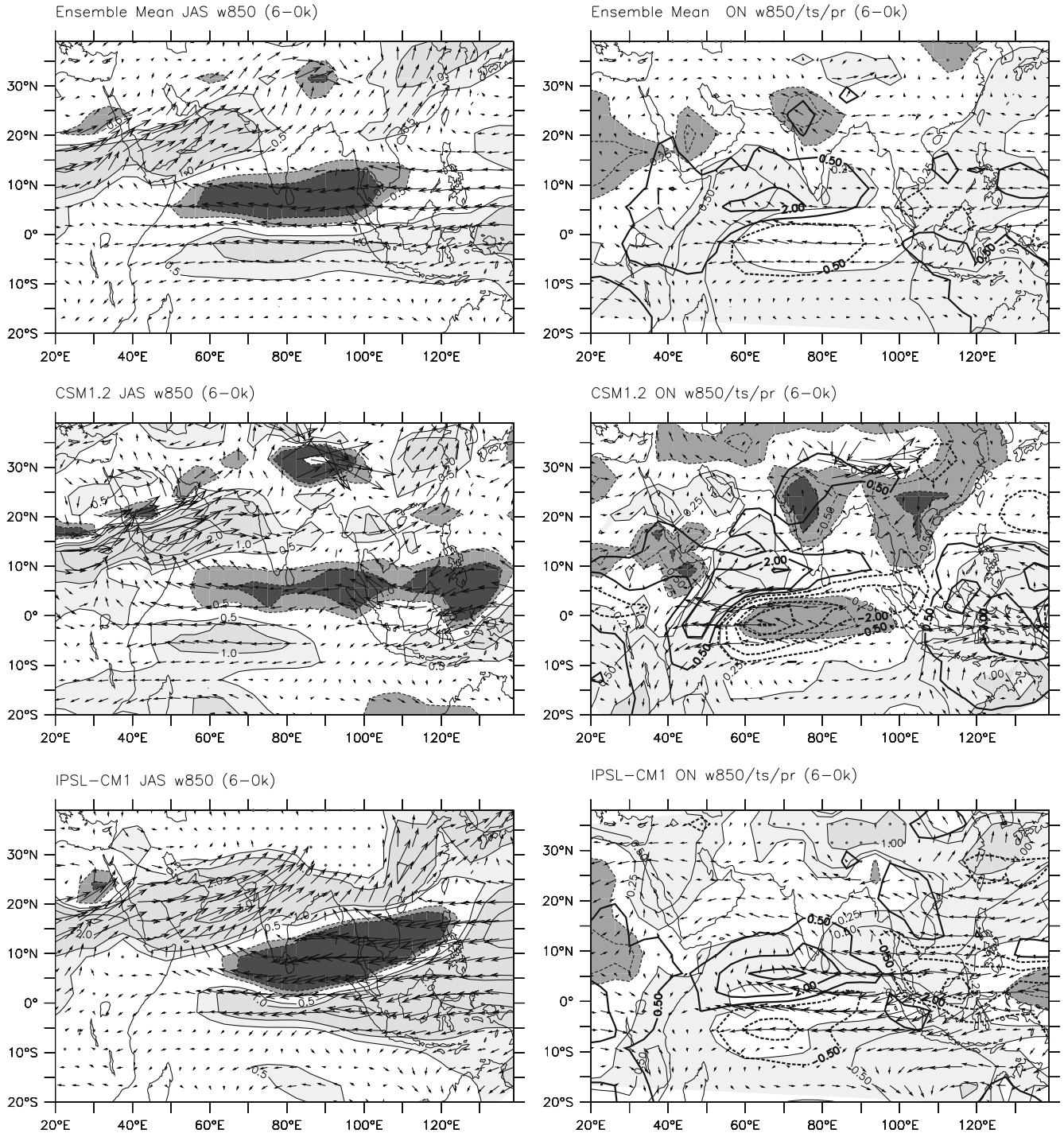

Fig. 12 Surface characteristics over the Indian sector as simulated by the six coupled models. Left: JAS differences between mid-Holocene and present 850 hPa wind (*arrows*) superimposed on the differences in 850 hPa wind speed. Isolines are plotted every 0.5 m/s. All arrows are referenced to the same scale. *Right* October–November (*ON*) differences between mid-Holocene and present 850 hPa wind (*arrows*) superimposed on the differences in SST. *Light (heavy) grey shading* indicates positive (negative) SST anomalies. The *thick black line* indicates where the increase in precipitation exceeds 0.5 mm/day, and the *thick black dotted line* where the reduction in precipitation exceeds 0.5 mm/day, the contour is 2 mm/day. Ensemble mean from six models (*top*) and two models CSM1.2 (*middle*) and IPSL-CM1 (*bottom*)

decreases during boreal autumn and winter and there is no obvious change during spring and summer. In IPSL-CM1, the variance decreases during late spring and early autumn. In MRI-CGCM1, the variance is weaker throughout the year, although the weakening is most marked during summer and autumn. None of the models show a significant change in the seasonality of maximum DMI activity; only the magnitude is af-

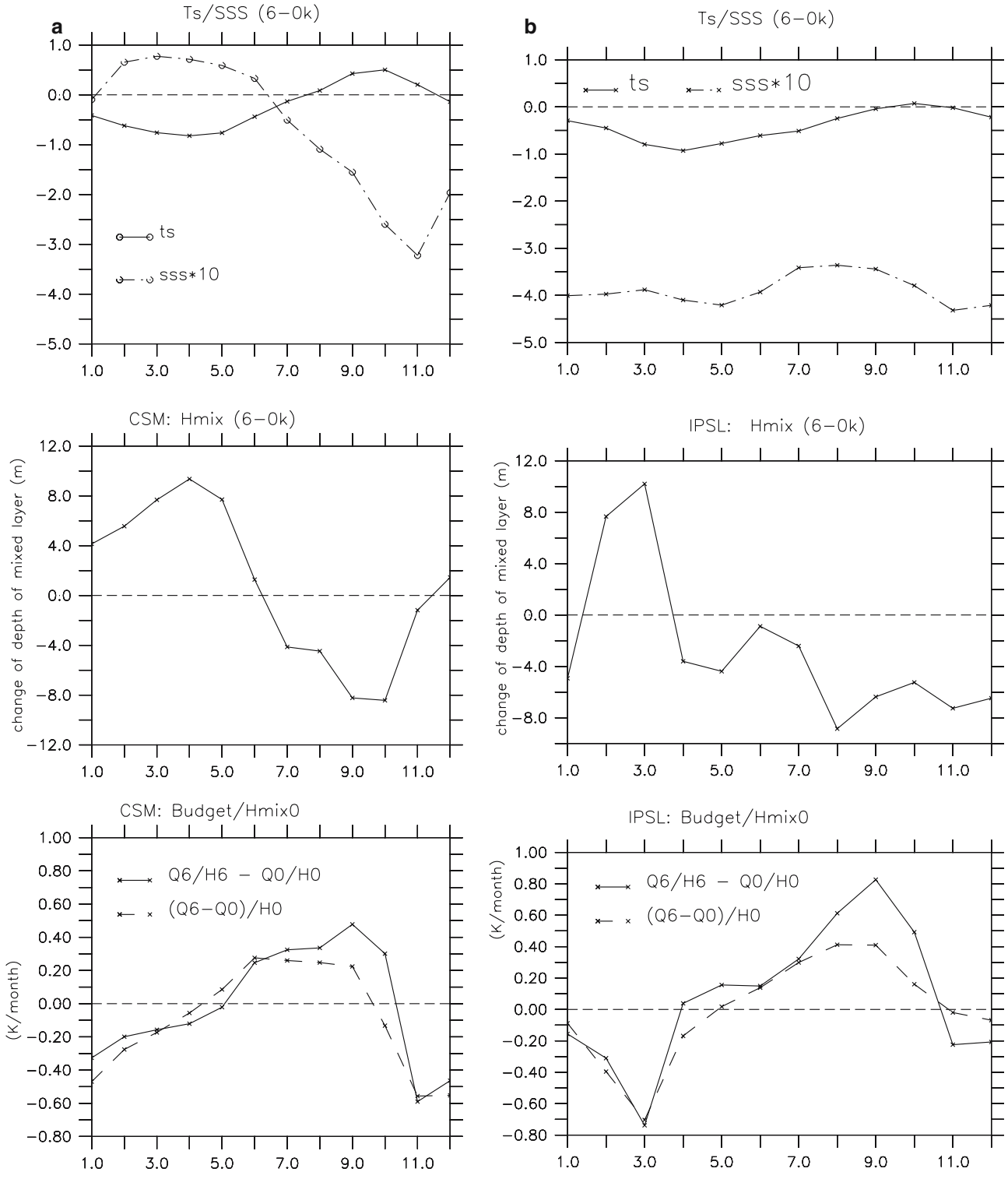

Fig. 13 Changes in mean monthly mean evolution of ocean surface variables for a box located in the northwestern Indian ocean (55–75°E, 5–15°N): **a** sea surface temperature (*solid line*, °C), sea surface salinity (*dashed-dotted line*, PSU), **c** mixed layer depth (m), and **d** comparison of the change in the surface rate of warming, when the change in mixed layer depth is neglected (*dashed line*) or considered (*solid line*). *Left* CSM1.2 model, *right* IPSL-CM1 model

fected. This suggests that the IOD was more stable during the mid-Holocene. The reinforcement of the IOD at the mean seasonal time scale thus damps the variability across the Indian Ocean.

We investigate the impact of this reduced variability on the large-scale patterns of the tropical convection. Since IOD events generally peak around October, we computed the correlation between the October–

November DMI and the outgoing longwave radiation (OLR) in order to estimate the impact of this reduced IOD variability on the large scale Walker and Hadley circulation across the Indian Ocean (Fig. 15b–e). Under modern conditions, IOD events are accompanied by a shift of deep convection (depicted by low OLR) towards the western part of the basin where SST is anomalously warm (Fig. 15a). For comparison, the correlation is also made for present day based on observed data with OLR data from the Climate Diagnostic Center, USA (http: //www.cdc.noaa.gov/) and DMI constructed with SST (http://www.emc.ncep.noaa.gov/research/cmb/sst_analysis/) covering the 1982–2003 period. The correlation pattern estimated from observed data is consistent with the reports of floods in east Africa and drought in Indonesia during IOD events. There is no statistically significant relationship with Indian rainfall.

All three models reproduce the broad pattern of this dipole correlation (Fig. 15b, d, e). However, the simulated correlation patterns are much weaker than the observed one for most models and the horseshoe structure is only partly represented. The dipole pattern can still be identified in the mid-Holocene simulation, but it is much weaker. The decrease in the relationship between IOD and OLR indicates that the interannual variability of deep convection related to the IOD was weaker during the mid-Holocene than at present. This suggests there were important changes in climate teleconnections during the mid-Holocene, and in the relative impact of ENSO and the IOD on the variability of the eastern part of the Indian Ocean.

5 Discussion and conclusions

We have analyzed the ocean response to mid-Holocene insolation using results from seven different coupled ocean-atmosphere models. Vegetation was prescribed to be the same as today in the coupled simulations, despite the fact that several studies have shown that the vegetation feedback enhances the insolation forcing in the tropics (Kutzbach et al. 1996; Claussen and Gayler 1997; Texier et al. 1997; Ganopolski et al. 1998; Broström et al. 1998; Braconnot et al. 1999; de Noblet-Ducoudre et al. 2000). The potential interaction between vegetation and ocean feedback, and the potential for further warming of the northern hemisphere mid-latitude oceans, needs to be evaluated carefully. However, the number of coupled simulations with interactive vegetation is still limited, whereas several coupled ocean-atmosphere simulations were available. This study should then be considered as a first step to better understand the response of the ocean to the insolation forcing and its feedback on the mid-Holocene climate.

Several robust changes in mean seasonal cycle and in climate variability have emerged from these analyses. The incorporation of ocean feedback introduces a slight delay in the response of the seasonal cycle to orbital forcing due to ocean inertia. Winter cooling and summer warming over the ocean therefore occur with one to two months delay compared to over the land. This has been noted in analyses of individual simulations (Kutzbach and Liu 1997; Hewitt and Mitchell 1998; Braconnot et al. 2000) and appears to be a consistent feature of the oceanic response to orbital forcing.

The delay in summer warming over the ocean reinforces monsoon activity both in western Africa and in the northwestern Indian Ocean. For Africa, the increased precipitation is associated with an increased Atlantic dipole structure with warmer temperature to

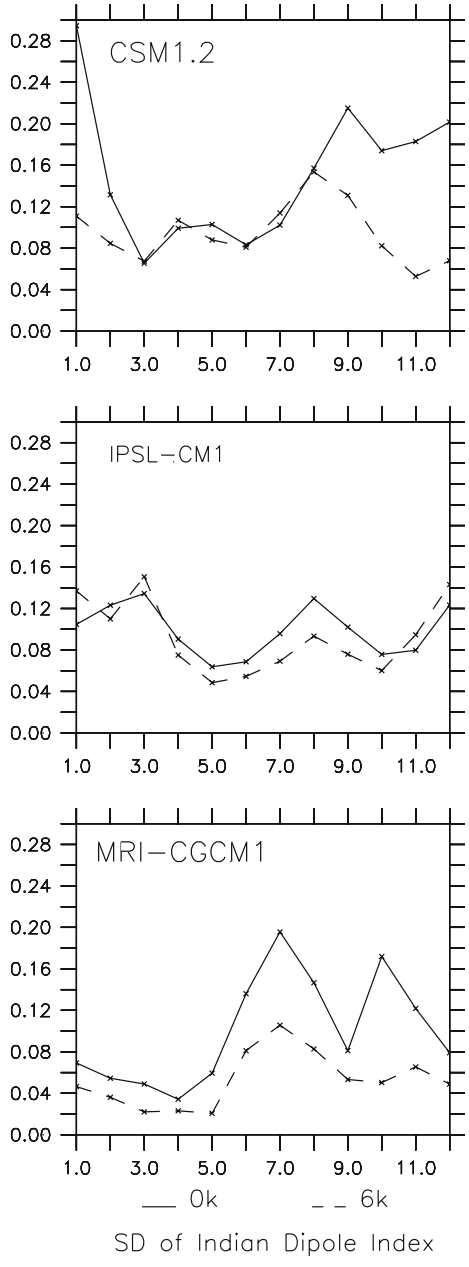

Fig. 14 Simulated monthly mean evolution of the Indian Dipole Index (*DPI*) for the present day climate (*solid line*) and the 6 ka climate (*dashed line*) for CSM1.2, IPSL-CM1 and MRI-CGCM1

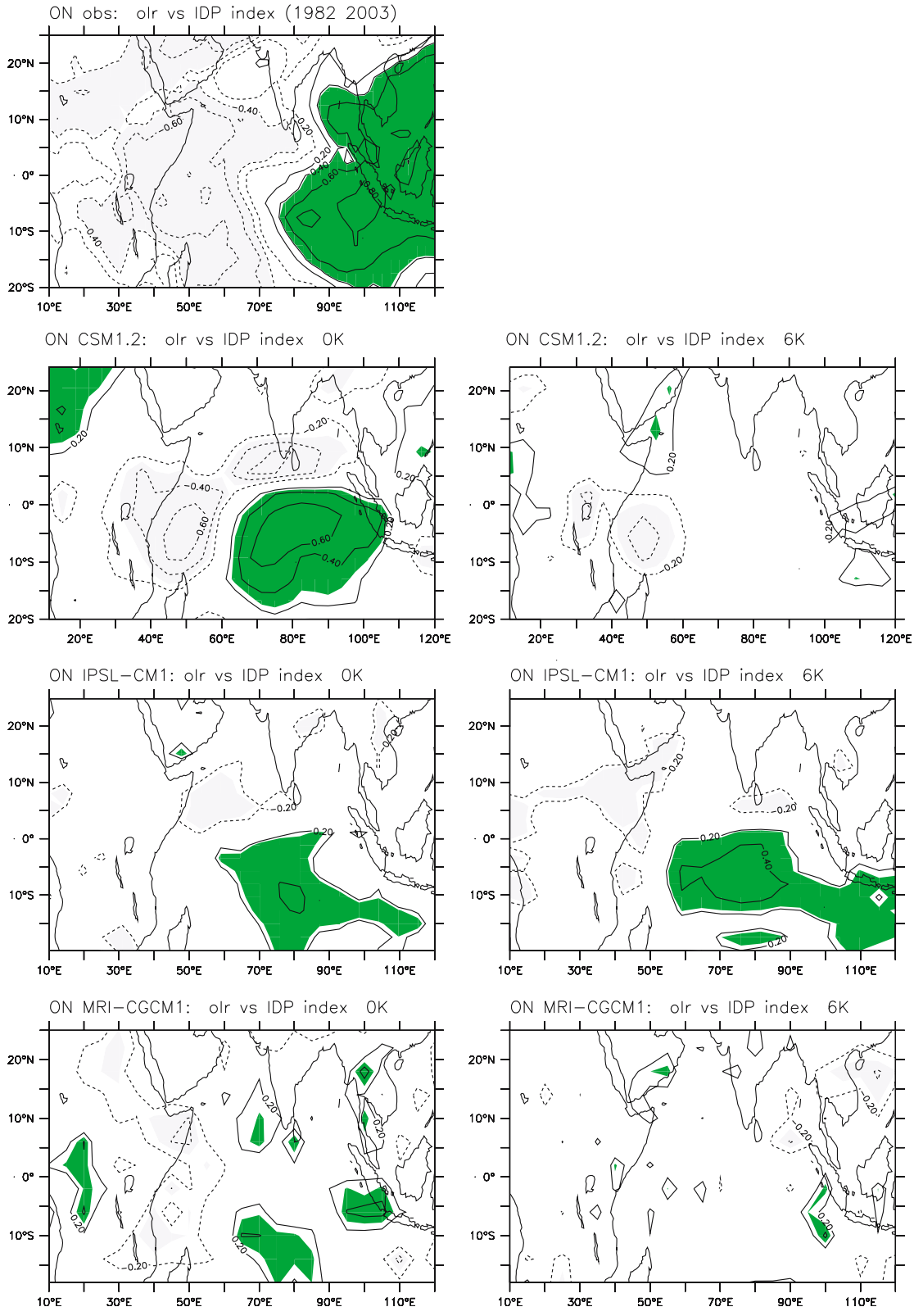

Fig. 15 Correlation patterns between DPI and OLR. **a** For OLR from NCEP/NCAR reanalysis and DPI from observed SST; **b**, **d** and **f** for CSM1.2, IPSL-CM1 and MRI-CGCM1 at present day, respectively; **c**, **e** and **g** for 6 ka. *Dark (light) grey shading* indicates a positive (negative) 5% level of significant. The 5% significant value is 0.42 for reanalysis and observed data; 0.28 for CSM1.2, 0.23 for IPSL-CM1 and 0.30 for MRI-CGCM1. Isolines are plotted every 0.20. *Solid line* is for positive value and dash line for negative value

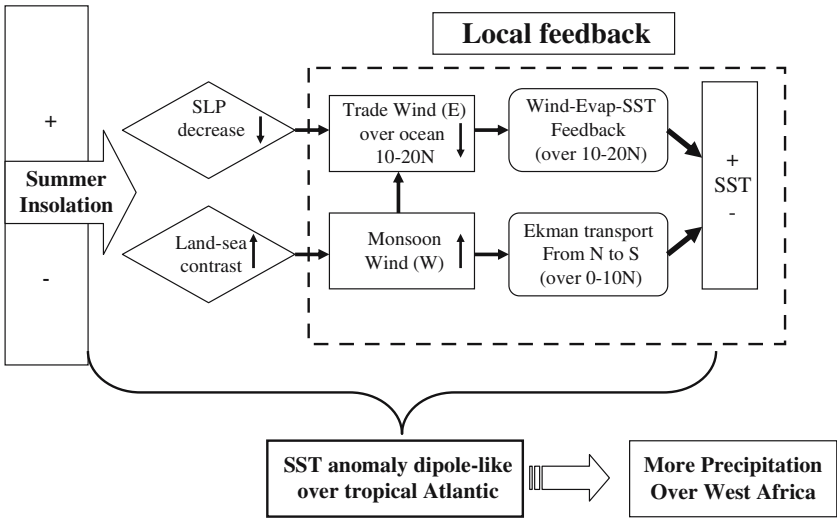

Fig. 16 Diagram schematic showing how the dipole structure of SST anomaly over tropical and subtropical Atlantic during boreal summer is created and maintained (see the text in details)

the north of 5°N and colder temperature to the south. This dipole is created by a combination of increased insolation and a strong wind-evaporation feedback around 15°N that leads to additional surface warming (Fig. 16). The monsoon trough deepens over these warm waters, which contributes to increase the inland advection of moisture with a northern position of the ITCZ. The system is also sustained by a southward Ekman drift, which delays the SST warming around 5°N and sharpens the dipole. The system relaxes when the warming of the southern hemisphere is sufficient to reverse the temperature gradient between the two hemispheres. In addition, late summer warming of the Mediterranean Sea and enhanced southward flow also contributes to increased precipitation over northern Africa (Rowell 2003; Tuenter et al. 2003). As a consequence, those models (CSM1.2, IPSL-CM1 and FOAM) that produce the largest shift in the southern position of the ITCZ over the ocean during winter and in the northern position of the ITCZ during summer, also produce the most pronounced dipole SST anomaly pattern over the Atlantic in JAS. This emphasizes the role of the interhemispheric temperature gradient in the shift of ITCZ across the tropical Atlantic.

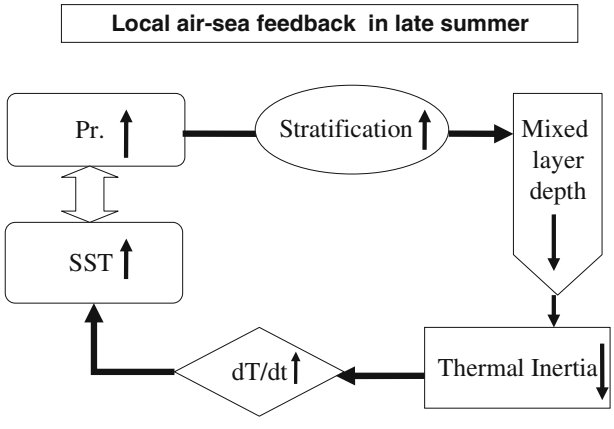

Fig. 17 Diagram schematic showing the local feedback over northwesten Indian ocean during late summer

Insolation and wind-evaporation feedback are also the primary reason for the late surface warming in the northwestern Indian Ocean. However, there is a more direct feedback between the wind convergence over the warm waters, increased precipitation and stratification of the surface ocean (Fig. 17). Variations of the mixed layer depth at this period of the year increase the rate of warming of the surface ocean. There is also some evidence that the stratification of the surface ocean is partly controlled by decreased salinity when precipitation is increased. However, models exhibit large differences in the simulated salinity fields. These differences may arise from the way the water budget is closed in the coupled simulations, which varies from the use of complex river-runoff schemes to ad-hoc solutions designed to conserve water globally. The influence of the method used to close the water budget on SSS should be investigated systematically in the PMIP II simulations.

In both the Atlantic and the Indian Ocean, mid-Holocene insolation leads to a reinforcement at the seasonal time scale of a dipole pattern and this has an impact on the characteristics of interannual variability in both western and eastern Africa. The coupled models produce a more consistent correlation between the sub-Saharian precipitation and the northern part of the dipole-like structure at interannual time scale during the mid-Holocene than for the present day. However, no significant change is detected in the way the Atlantic dipole varies at the interannual time scale. This suggests there was a change in the teleconnection between western Africa and the Atlantic Ocean. In the Indian sector, on the other hand, the increase in the IOD at the seasonal time scale damps interannual variability and this results in a reduction of the teleconnection pattern with OLR.

Further analyses are required to understand and evaluate the changes in interannual variability and the

relative impact of SST in the different equatorial basins. Although changes in e.g. ENSO variability have been inferred from coral records (Tudhope et al. 2001), more annually-resolved records are required to evaluate whether the simulated patterns of change in variability are realistic. Given that there are different regional responses, a network of coral records across the tropics, combined with records from annually-laminated marine and coastal sediments, would be useful. Rimbu et al. (2004) have shown that increases in tropical SST are accompanied by a decrease of SST in the eastern North Atlantic at multi-decadal time scales. Note that we have not investigated ENSO variability in this study because it was poorly represented in the coupled model under modern conditions and an initial examination didn't allow us to found robust features like the ones found for the Atlantic or the Indian sectors. It is hoped that new model versions and the longer simulations being carried out in PMIP II will make such analyses possible.

Our analyses also make it clear that evaluating model simulations of ocean conditions during the mid-Holocene will make stringent demands on palaeoenvironmental data synthesis. Relatively small changes in the timing of the mean seasonal cycle of SSTs and in the magnitude of SST changes in key regions have a large impact on the location of the monsoon front and hence regional precipitation patterns. Existing syntheses of SST data for the mid-Holocene are inadequate to distinguish between simulated SST fields, particularly given that the changes relative to today are small. Slow sedimentation rate over much of the ocean means that it is difficult to separate a distinct 6,000 years BP sample. The most comprehensive data set currently available for the mid-Holocene is that of Ruddiman and Mix (1993). This data set only covers the North Atlantic, and the samples likely reflect a long-term average of mid-Holocene conditions. The reconstruction of marine conditions along the coast of Africa and in the Indian ocean made by Texier et al. (2000) is biased towards early Holocene conditions. Liu et al. (2003) have compiled marine data representative of the difference between the period 10–5 kyr BP relative to the period 5–0 kyr BP. However, several reconstructions from high sediment rate records are now available (e.g. Wang et al. 1999; de Menocal et al. 2000). It may be possible to evaluate coupled simulations more rigorously in the future. We thus leave as a central part of the work carried out in the second phase of PMIP the systematic analysis of the role of the ocean and vegetation feedbacks on the mid-Holocene mean climate and climate variability, and their careful evaluation against palaeo indicators.

Acknowledgements This work was supported by the European funded project MOTIF (EVK2-CT-2002-00153), and from the French Programm national d'etude du climat ECHO. We would like to thank Jean-Yves Peterschmitt for his help with the model fields. This paper is a contribution from the PMIPI working group on coupled simulations.

References

Braconnot P, Joussaume S, Marti O, de Noblet N (1999) Synergistic feedbacks from ocean and vegetation on the African monsoon response to mid-Holocene insolation. Geophys Res Lett 26:2481–2484

Braconnot P, Marti O, Joussaume S, Leclainche Y (2000) Ocean feedback in response to 6 kyr BP insolation. J Clim 13:1537–1553

Braconnot P, Loutre MF, Dong B, Joussaume S, Valdes P (2002) How the simulated change in monsoon at 6 ka BP is related to the simulation of the modern climate: results from the Paleoclimate Modeling Intercomparison Project. Clim Dyn 19:107–121

Braconnot P, Joussaume J, Harrison S, Hewitt C, Valdes P, Ramstein G, Stouffer RJ, Otto-Bleisner BL, Taylor KE (2003) The second phase of the Paleoclimate Modeling Intercomparison Project (PMIP II). Clivar Exchanges 8:19–20

Braconnot P, Marti O (2003) Impact of precession on monsoon characteristics from coupled ocean atmosphere experiments: changes in Indian monsoon and Indian ocean climatology. Mar Geol 201:23–34

Braconnot P (2004) Modeling the last glacial maximum and mid-holocene. Comptes Rendus Geosci 336:711–719

Braconnot P, Harrison S, Joussaume J, Hewitt C, Kitoh A, Kutzbach J, Liu Z, Otto-Bleisner BL, Syktus J, Weber SL (2004) Evaluation of coupled ocean-atmosphere simulations of the mid-Holocene. In: Batterbee et al (ed) Past climate variability through Europe and Africa. Kluwer, Dordrecht

Broström A, Coe MT, Harrison SP, Gallimore RG, Kutzbach JE, Foley J, Prentice CI, Behling P (1998) Land surface feedbacks and paleomonsoons in northern Africa. Geophys Res Lett 25:3615–3618

Chang P, Ji L, Li H (1997) A decadal climate variation in the tropical Atlantic Ocean from thermodynamic air–sea interactions. Nature 385:516–518

Chang P, Saravanan R, Ji L, Hegerl GC (2000) The effect of local sea surface temperatures on atmospheric circulation over the tropical Atlantic sector. J Clim 13:2195–2216

Claussen M, Gayler V (1997) The greening of the Sahara during the mid-Holocene: results of an interactive atmosphere-biome model. Global Ecol Biogeogr Lett 6:369–377

Clemens SC, Prell WL (2003) A 350,000 year summer-monsoon multi-proxy stack from the Owen ridge, Northern Arabian sea. Mar Geol 201:35–51

Coe MT, Harrison SP (2002) The water balance of northern Africa during the mid-Holocene: an evaluation of the 6 ka BPPMIP simulations. Clim Dyn 19:155–166

COHMAP-Members (1988) Climatic changes of the last 18,000 years: observations and model simulations. Science 241:1043–1052

Davey MK, Huddleston M, Sperber KR, Braconnot P, Bryan F, Chen D, Colman A, Cooper C, Cubasch U, Delecluse P, De Witt D, Fairhead L, Flato G, Gordon C, Hogan T, Ji M, Kimoto M, Kitoh A, Knutson T, Latif M, Le Treut H, Li T, Manabe S, Mechoso C, Meehl GA, Oberhuber J, Power S, Roeckner E, Terray L, Vintzileos A, Voss R, Wang B, Washington WM, Yoshikawa I, Yu J-Y, Yukimoto S, Zebiak S (2002) STOIC: a study of coupled model climatology and variabiity in tropical ocean regions. Clim Dyn 18:403–420

de Noblet-Ducoudre N, Claussen R, Prentice C (2000) Mid-Holocene greening of the Sahara: first results of the GAIM 6000 year BP Experiment with two asynchronously coupled atmosphere/biome models. Clim Dyn 16:643–659

deMenocal P, Ortiz J, Guilderson T, Sarnthein M (2000) Coherent high- and low-latitude climate variability during the holocene warm period. Science 288:2198–2202

Folland CK, Palmer TN, Parker DE (1986) Sahel rainfall and world wide sea surface temperature. Nature 320:602–607

Fontaine B, Janicot S (1996) Sea surface temperature fields associated with West African rainfall anomaly types. J Clim 9:2935–2940

Gadgil S, Sajani S (1998) Monsoon precipitation in the AMIP runs. Clim Dyn 14:659–689

Gadgil S, Vinayachandran PN, Francis PA (2003) Droughts of the Indian summer monsoon: Role of clouds over the Indian Ocean. Curr Sci 85:1713–1719

Ganopolski A, Kubatzki C, Claussen M, Brovkin V, Petoukhov V (1998) The influence of vegetation-atmosphere–ocean interaction on climate during the mid-Holocene. Science 280:1916–1919

HadISST (2003) J Geophys Res 108:4407. DOI 10.1029/2002JD002670

Harrison S, Braconnot P, Hewitt C, Stouffer RJ (2002) Fourth international workshop of The Palaeoclimate Modelling Intercomparison Project (PMIP): launching PMIP Phase II. EOS 83:447–447

Harrison SP, Jolly D, Laarif F, Abe-Ouchi A, Dong B, Herterich K, Hewitt C, Joussaume S, Kutzbach JE, Mitchell J, de Noblet N, Valdes P (1998) Intercomparison of simulated global vegetation distributions in response to 6 kyr BP orbital forcing. J Clim 11:2721–2742

Harrison SP, Kutzbach JE, Liu Z, Bartlein PJ, Otto-Bliesner B, Muhs D, Prentice IC, Thompson RS (2003) Mid-Holocene climates of the Americas: a dynamical response to changed seasonality. Clim Dyn 20:663–688

Hewitt CD, Mitchell JFB (1998) A fully coupled GCM simulation of the climate of the mid-Holocene. Geophys Res Lett 25:361–364

Hoelzmann P, JollyD, Harrison SP, Laarif F, Bonnefille R, Pachur H-J (1998) Mid-Holocene land-surface conditions in northern Africa and the Arabian peninsula: a data set for AGCM simulations. Global Biogeochem Cycles 12:35–52

Jacob RL (1997) Low frequency variability in a simulated atmosphere oceansystem. PhD thesis, University of Wisconsin–Madison, pp 170

Janicot S (1992) Spatio-temporal variability of West African rainfall. Part I: Regionalisation and typing. J Clim 5:489–497

Janicot S, Moron V, Fontaine B (1996) Sahel droughts and ENSO dynamics. Geophys Res Lett 23:515–518

Jolly D, Harrison SP, Damnati B, Bonnefille R (1998) Simulated climate and biomes of Africa during the Late Quaternary: comparison with pollen and lake status data. Quaternary Sci Rev 17:629–657

Joussaume S, Taylor KE (1995) Status of the Paleoclimate Modeling Intercomparison Project. In: Proceedings of the first international AMIP scientific conference, WCRP-92, Monterey, pp 425–430

Joussaume S, Taylor KE, Braconnot P, Mitchell JFB, Kutzbach JE, Harrison SP, Prentice IC, Broccoli AJ, Abe-Ouchi A, Bartlein PJ, Bonfils C, Dong B, Guiot J, Herterich K, Hewitt CD, Jolly D, Kim JW, Kislov A, Kitoh A, Loutre MF, Masson V, McAvaney B, McFarlane N, de Noblet N, Peltier WR, Peterschmitt JY, Pollard D, Rind D, Royer JF, Schlesinger ME, Syktus J, Thompson S, Valdes P, Vettoretti G, Webb RS, Wyputta U (1999) Monsoon changes for 6000 years ago: results of 18 simulations from the Paleoclimate Modeling Intercomparison Project (PMIP). Geophys Res Lett 26:859–862

Kitoh A, Murakami S (2002) Tropical Pacific climate at the mid-Holocene and the last glacial maximum simulated by a coupled ocean-atmosphere general circulation model. Paleoceanography 17(3):1047

Kohfeld KE, Harrison SP (2000) How well can we simulate past climates? Evaluating the models using global palaeoenvironmental datasets. Quaternary Sci Rev 19:321–346

Kutzbach JE, Otto-Bliesner BL (1982) The sensitivity of the African-Asian monsoon climate to orbital parameter changes for 9000 years B. P. in a low- resolution general circulation model. J Atmos Sci 39:1177–1188

Kutzbach JE, Street-Perrot FA (1985) Milankovitch forcing of fluctuations in the level of tropical lakes from 18 to 0 kyr BP. Nature 317:130–134

Kutzbach JE, Bartlein PJ, Foley JA, Harrison SP, Hostetler SW, Liu Z, Prentice IC, Webb T (1996) Potential role of vegetation feedback in the climate sensitivity of high-latitude regions: a case study at 6000 years BP. Global Biogeochem Cycles 10:727–736

Kutzbach JE, Liu Z (1997) Response of the African monsoon to orbital forcing and ocean feedbacks in the middle Holocene. Science 278:440–443

Lamb JP, Peppler RA (1992) Further case studies of Tropical Atlantic surface atmospheric and oceanic patterns associated with Sub-Sahara Drought. J Clim 5:476–488

Latif M, Sperber K, Arblaster J, Braconnot P, Chen D, Colman A, Cubasch U, Cooper C, Delecluse P, DeWitt D, Fairhead L, Flato G, Hogan T, Ji M, Kimoto M, Kitoh A, Knutson T, Le Treut H, Li T, Manabe S, Marti O, Mechoso C, Meehl G, Power S, Roeckner E, Sirven J, Terray L, Vintzileos A, Voss R, Wang B, Washington W, Yoshikawa I, Yu J, Zebiak S (2001) ENSIP: the El Nino simulation intercomparison project. Clim Dyn 18:255–276

Liu Z, Jacob R, Kutzbach J, Wu L, Anderson J, Harrison S (2000) Monsoon impact on El-Niño in the Early Holocene. In: Braconnot P (ed)Paleoclimate modeling Intercomparison Project (PMIP), proccedings of the third PMIP Workshop, pp 205–209

Liu Z, Brady EC, Lynch-Stieglitz (2003) Global ocean response to orbital foring in the Holocene. Paleoceanography 18:1041

Nicholson SE, Grist JP (2001) A conceptual model for understanding rainfall variability in the West African Sahel on interannual and interdecadal timescales. Int J Climatol 21:1733–1757

Otto-Bliesner BL (1999) El Nino La Nina and Sahel precipitation during the middle Holocene. Geophys Res Lett 26:87–90

PMIP (2000) Paleoclimate Modeling Intercomparison Project (PMIP), proceedings of the third PMIP Workshop. WCRP-111,WMO/TD-No. 1007, 271 pp

Reynolds RW (1988) A real time global sea-surface temperature analysis. J Clim 1:75–86

Rimbu N, Lohmann G, Lorenz SJ, Kim JH, Schneider RR (2004) Holocene climate variability as derived from alkenone sea surface temperature and coupled ocean–atmosphere model experiments. Clim Dyn 23:215–227

Rowell DP (2003) The impact of Mediterranean SSTs on the Sahelian rainfall season. J Clim 16:849–862

Ruddiman WF, Mix AC (1993) The north and equatorial Atlantic at 9000 and 6000 yr BP. In: Wright HEJ, Kutzbach JE, Webb T III, Ruddiman WF, Street-Perrott FA, Bartlein PJ (eds) Global climates since the last glacial maximum. University of Minnesota Press, Minnesota, pp 94–124

Saji NH, Goswami BN, Vinayachandran PN, Yamagata Y (1999) A dipole mode in the tropical Indian Ocean. Nature 401:360–363

Street FA, Grove AT (1976) Environmental and climatic implications of late Quaternary lake-level fluctuations in Africa. Nature 261:385–390

Street-Perrott FA, Perrott RA (1993) Holocene vegetation, lake levels and climate of Africa. In: Wright HEJ, Kutzbach JE, Webb T III, Ruddiman WF, Street-Perrott FA, Bartlein PJ (eds) Global Climates since the Last Glacial Maximum. University of Minnesota Press, Minnesota, pp 318–356

Tao SY, Chen LX (1987) A review of recent research on the East Asian summer monsoon in China. In: Chang CP, Krishnamurti TN (eds) Monsoon meteorology. Oxford University Press, Oxford, pp 60–92

Texier D, de Noblet N, Harrison SP, Haxeltine A, Jolly D, Joussaume S, Laarif F, Prentice IC, Tarasov P (1997) Quantifying the role of biosphere-atmosphere feedbacks in climate change: coupled model simulations for 6000 years BP and comparison with palaeodata for northern Eurasia and northern Africa. Clim Dyn 13:865–882

Texier D, de Noblet N, Braconnot P (2000) Sensitivity of the African and Asian monsoons to mid-Holocene insolation and data-inferred surface changes. J Clim 13:164–181

Tudhope AW, Chilcott CP, McCulloch MT, Cook ER, Chappell J, Ellam RM, Lea DW, Lough JM, Shimmield GB (2001) Vari-

ability in the El Nino—Southern oscillation through a glacial-interglacial cycle. Science 291:1511–1517

Tuenter E, Weber SL, Hilgen FJ, Lourens LJ (2003) The response of the African summer monsoon to remote and local forcing due to precession and obliquity. Global Planet Change 36:219–235

Vizy EK, Cook KH (2001) Mechanisms by which Gulf of Guinea and eastern North Atlantic sea surface temperature anomalies can influence African rainfall. J Clim 14:795–821

Voss R, Mikolajewicz U (2001 The climate 6000 years BP in near-equilibrium simulations with a coupled AOGCM. Geophys Res Lett 28:2213–2216

Wang L, Sarnthein M, Erlenkeuser H, Grimalt J, Grootes P, Heilig S, Ivanova E, Kienast M, Pelejero C, Pflaumann U (1999) East Asian monsoon climate during the Late Pleistocene: high-resolution sediment records from the south China Sea. Mar Geol 156:245–284

Weber SL (2001) The impact of orbital forcing on the climate of an intermediate-complexity coupled model. Global Planet Change 30(1–2):7–12

Webster PJ, Moore AM, Loschnigg JP, Leben RR (1999) Coupled ocean–atmosphere dynamics in the Indian Ocean during 1997–1998. Nature 401:356–360

Wohlfahrt J, Harrison SP, Braconnot P (2004) Synergistic feedbacks between ocean and vegetation on mid- and high-latitude climates during the mid-Holocene. Clim Dyn 22:223–238

Yu G, Harrison SP (1996) An evaluation of the simulated water balance of Eurasia and northern Africa at 6000 y BP using lake status data. Clim Dyn 12:723–735

Yu G, Prentice CI, Harrison SP, Sun X (1998) Pollen-based reconstructions for China for 0 ka and 6 ka. J Biogeogr 25:1055–1069

Zhang Y, Sperber KR, Boyle JS, Dix M, Ferranti L, Kitoh A, Lau KM, Miyakoda K, Randall D, Takacs L, Wetherald R (1997) East Asian winter monsoon: results from eight AMIP models. Clim Dyn 13:797–820